TECHNISCHE
UNIVERSITÄT
WIEN
Vienna University of Technology

DIPLOMARBEIT

Coordinated Scheduling and Beamforming in Coordinated Multi-Point Transmission Systems

Ausgeführt zum Zwecke der Erlangung des akademischen Grades eines
Diplom-Ingineurs

unter der Leitung von

Univ.Prof. Dipl.-Ing. Dr.techn. Markus Rupp
Dipl.-Ing. Dr.techn. Stefan Schwarz

Institute of Telecommunications

eingereicht an der Technischen Universität Wien
Fakultät für Elektrotechnik und Informationstechnik

von

Sana Žunić
Matrikelnr.: 0627758
Stolberggasse 42/3A
1050 Wien

Wien, Juni 2014

Abstract

Wireless cellular networks are currently experiencing a tremendous growth of data traffic. The resulting network densification leads to ever-increasing levels of Inter-Cell Interference (ICI) that cannot be managed with (semi)-static interference-avoidance schemes deployed in 3GPP Long Term Evolution (LTE) systems. Coordinated Multi-Point (CoMP) transmission is therefore adopted in LTE Advanced, the next development stage of LTE. The basic idea of CoMP is to enhance network performance by mitigating ICI through cooperation between several network cells.

Among the CoMP schemes, Coordinated Beamforming (CB) and Coordinated Scheduling (CS) stand out, as they do not rely on the exchange of user data between network nodes and thereby avoid additional network overhead. Instead, the network nodes coordinate their scheduling decisions and precoder design in order to minimize ICI and increase system throughput, especially at the cell edge. During the last decade, a multitude of algorithms achieving this objective has been proposed. But until now, no systematic study of their performance has been conducted.

This thesis aims to characterize and evaluate the performance of multiple proposed CB and CS schemes in a downlink multi-cell system. First, the fundamentals of LTE-A as well as the system model are introduced. CB is described next, CB algorithms are derived and evaluated by means of Monte Carlo simulations. The concept of CS is outlined, followed by a detailed description of a CS algorithm and Monte Carlo simulations. Besides throughput and spectral efficiency, fairness is also taken into account. The simulation results show that CoMP transmission significantly improves the system performance.

Contents

Chapter 1

Introduction

Data traffic in wireless cellular networks has increased considerably during the last decade, and the growth is expected to continue [1]. Figure 1.1 shows the predicted eleven-fold increase of mobile data traffic over the next four years. The cause of this exponential growth are modern mobile devices, in particular smartphones and tablets. In order to limit the traffic load per network node, a denser network deployment is necessary. However, this comes at the price of increased Inter-Cell Interference (ICI) which significantly degrades the network performance, especially at the cell edge. Unlike in the central area of the cell, User Equipments (UEs) at the cell boundary suffer from high interference power caused by neighboring cells.

In cellular networks, ICI has been an issue for many years. Traditionally, to mitigate the interference between them, the neighboring cells used different parts of the frequency spectrum and the frequency was reused at cells that were distanced
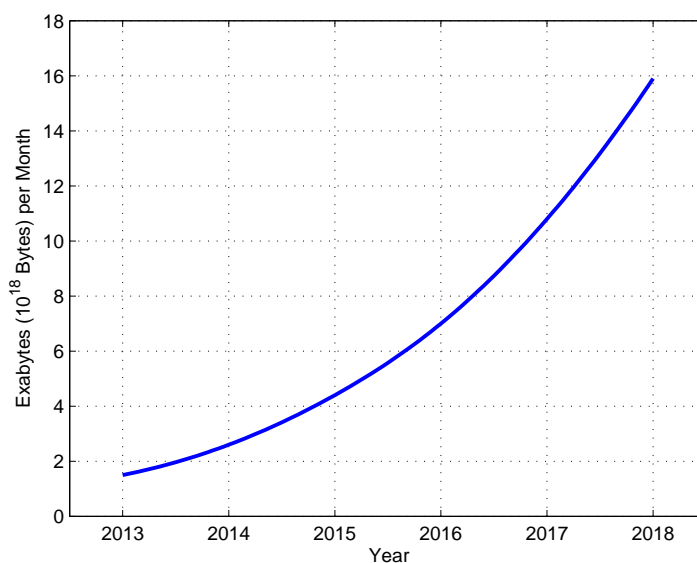

Figure 1.1: Estimated growth of mobile data traffic [1].

1

far enough.   However, the main drawback of frequency reuse is a poor spectral efficiency. Since frequency spectrum is a scarce resource and needs to be utilized efficiently, cells in Long Term Evolution (LTE) systems all share the same spectrum. To reduce interference between cells, LTE Release 8 introduces a coordination mechanism called ICI Coordination (ICIC) [2]. It allows neighboring base stations, i.e. eNodeBs in 3GPP terminology, to jointly allocate resources to their cell-edge UEs. The exchange of interference-coordination information between eNodeBs (eNBs) is supported by a standardized interface named X2.

Interest in interference coordination methods has significantly grown in recent years.   Consequently, the methods have evolved from simple (semi)-static ICIC to dynamic cooperation schemes, such as Coordinated Multi-Point (CoMP) transmission. CoMP relies on cooperation between eNBs to enhance the cell-edge UE throughput in particular, but also the average system throughput [3, 4]. This is achieved by either avoiding or exploiting ICI. After comprehensive study, 3GPP adopted CoMP as one of the key features in LTE-A Release 11 [5]. The CoMP transmission schemes considered in Release 11 can be classified as Joint Processing (JP), Coordinated Scheduling (CS) and Coordinated Beamforming (CB).

The idea of CB goes back to the work of [6], where the beamforming coefficients and power levels are calculated to satisfy a set of target Signal-to-Interference-plus-Noise Ratios (SINRs) for a given set of transmission links. Deployment of CS in cellular networks was proposed later. Initially, CS was considered for systems where cells are grouped in clusters so that eNBs within a cluster can jointly schedule transmissions to their UEs [7]. In recent works CS and CB are used as a tool to reduce ICI [8, 9, 10]. Unlike JT, these techniques rely only on the exchange of control information among eNBs and don't require user data exchange. For this reason, CS and CB are considered more suitable for practical implementation.

This master thesis investigates basic principles of CS and CB, as well as their capability to remove ICI and so improve the network performance. A systematic comparison between different scheduling and beamforming algorithms is provided. The focus of the thesis lies on homogeneous cellular networks with only one UE per cell served simultaneously. The network eNBs are capable of coordinating their scheduling decisions and precoder designs. In order to evaluate and compare the performance of the presented algorithms, the Vienna LTE-A Link Level Simulator, a standard-compliant Matlab-based simulator [11, 12], is utilized. Note that simulations are necessary to test and optimize algorithms prior to their implementation.

Following this introductory chapter, Chapter 2 gives an overview of LTE-A, in particular the physical and Medium Access Control (MAC) layer, and introduces the system model. It provides the theoretical and mathematical basis for the anal-

yses conducted in later chapters. A detailed study of Coordinated Beamforming is carried out in Chapter 3. It presents the beamforming algorithms and discusses their performance in terms of throughput and spectral efficiency for different simulation scenarios. Chapter 4 then examines Coordinated Scheduling. The scheduling algorithm is described in detail and the obtained simulation results are analyzed with respect to throughput and fairness. Chapter 5 finally concludes the work and gives an outlook on possible future research areas.

The following notation is used throughout this thesis. $\mathbb{E}\{x\}$ denotes the expected value of a random variable x. Vectors are represented in lowercase boldface letters, matrices using uppercase boldface letters. Terms $\mathbf{a}^*$ and $\|\mathbf{a}\|$ refer to the complex conjugate and Euclidean norm of vector $\mathbf{a}$, respectively. $\mathbf{A}^H$, $\mathbf{A}^{-1}$, $\text{tr}(\mathbf{A})$ and $\|\mathbf{A}\|_F$ stand for the conjugate transpose, inverse, trace and Forbenius norm of matrix $\mathbf{A}$, respectively. Vector $\mathbf{v}_{max,i}\{\mathbf{A}\}$ denotes the eigenvector of $\mathbf{A}$ corresponding to the i-th largest eigenvalue. $\mathbf{I}_r$ represents an $r \times r$ identity matrix and $\mathbf{0}_{r \times s}$ denotes an $r \times s$ zero matrix.

Chapter 2

Theoretical Background

2.1 LTE-(A) Overview

LTE-A is an enhancement of LTE developed by 3GPP in Release 10 and beyond. Therefore, LTE-A shares the technological fundamentals of LTE. The relevant physical and MAC layer aspects of this technology are discussed in the following.

2.1.1 MIMO OFDM Transmission

The radio transmission in LTE downlink is based on Orthogonal Frequency Division Multiplexing (OFDM), which converts the broadband frequency-selective wireless channel into multiple orthogonal frequency-flat subchannels, called subcarriers [13]. Subcarriers are organized in sets of twelve consecutive subcarriers. Figure 2.1 illustrates the transmission structure for the Frequency Division Duplex (FDD) mode considered in this thesis. In the time domain, a radio frame of length 10 ms is divided into ten subframes of 1 ms duration each. Every subframe consists of two equally sized slots with seven OFDM symbols per slot. One subcarrier during one OFDM symbol interval constitutes a Resource Element (RE), the smallest unit for data transmission. In order to keep the signaling overhead manageable, feedback is provided in Resource Block (RB) granularity. As shown in Figure 2.1, an RB consists of one 0.5 ms slot (seven OFDM symbols) in the time domain and one subcarrier set (twelve subcarriers) in the frequency domain, i.e. $7 \times 12 = 84$ REs. Note that this resource structure is valid for the normal-length cyclic prefix and 15 kHz subcarrier spacing.

Every RB is uniquely identified by the pair $[\eta, \kappa]$ where η and κ represent indices of the slot and the subcarrier set, respectively. Similarly, each RE of a specific RB $[\eta, \kappa]$ is identified by the pair $[n, k]$, where $n \in \{7\eta - 6, 7\eta - 5, \ldots, 7\eta\}$ is the time-symbol index and $k \in \{12\kappa - 11, 12\kappa - 10, \ldots, 12\kappa\}$ is the subcarrier index. The
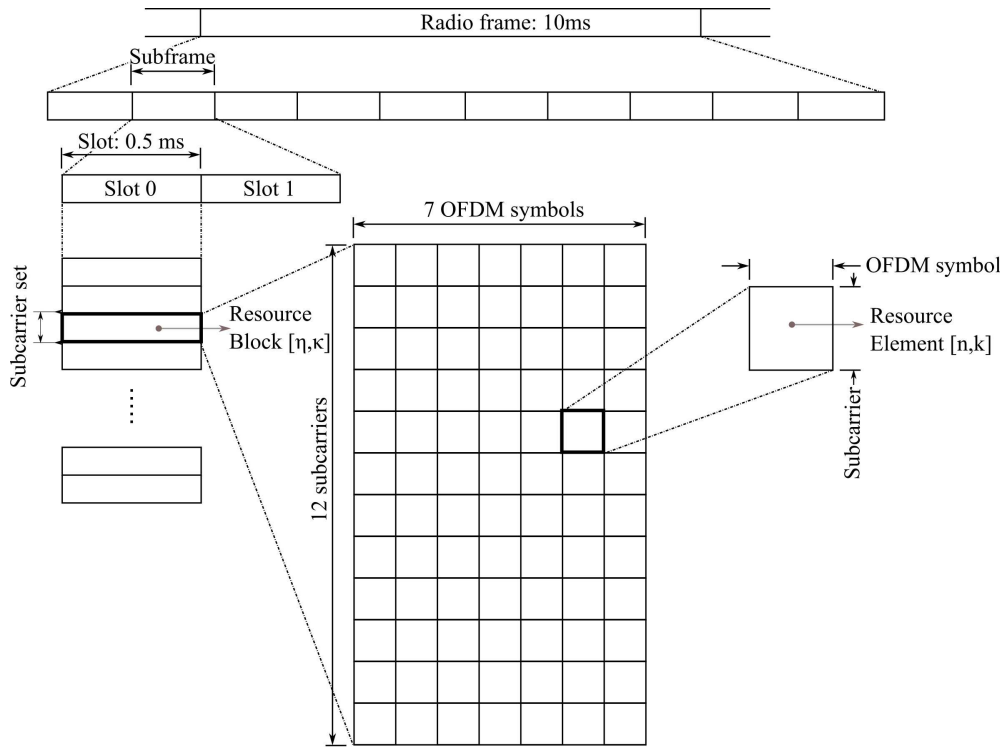
Figure 2.1: LTE time-frequency resource structure [14, 15].

relation between the index pairs $[\eta, \kappa]$ and $[n, k]$ is therefore given by

$$\eta = \left\lceil \frac{n}{7} \right\rceil , \, \kappa = \left\lceil \frac{k}{12} \right\rceil . \tag{2.1}$$

The amount of RBs available for transmission depends on the allocated bandwidth. The available channel bandwidths as well as the resulting number of RBs and subcarriers defined in the LTE standard are listed in Table 2.1.

LTE supports the application of multiple transmit antennas at the eNB and multiple receive antennas at the UE, thus enabling the Multiple Input Multiple Output (MIMO) transmission. The additional antennas can be used as a tool to further improve SINR and achieve higher diversity gain compared to the use of a single transmit antenna or a single receive antenna. However, there is also the possibility of multiplexing several transmissions in the spatial domain. The spatial multiplexing allows parallel transmissions of multiple data streams, termed

Channel bandwidth [MHz]	1.4	3	5	10	15	20
Number of Resource Blocks	6	15	25	50	75	100
Number of subcarriers	72	180	300	600	900	1200

Table 2.1: LTE system bandwidths and available resources [16].

spatial layers, on the same RB. This provides an additional multiplexing gain, but introduces interference between the spatial layers as well. LTE-A defines support for up to eight transmit antennas, enabling up to eight-layer spatial multiplexing in the downlink.

Figure 2.2 schematically illustrates the physical layer processing of user data at the eNB. Within each Transmission Time Interval (TTI), corresponding to one subframe, up to two transport blocks of dynamic size are delivered to the physical layer, processed and transmitted. Channel coding and modulation are performed first, generating complex-valued modulated symbols. The eNB can dynamically adjust the applied code rate and modulation scheme and so adapt to quality variations of the transmission link. The process of link adaptation is detailed in Section 2.1.2.
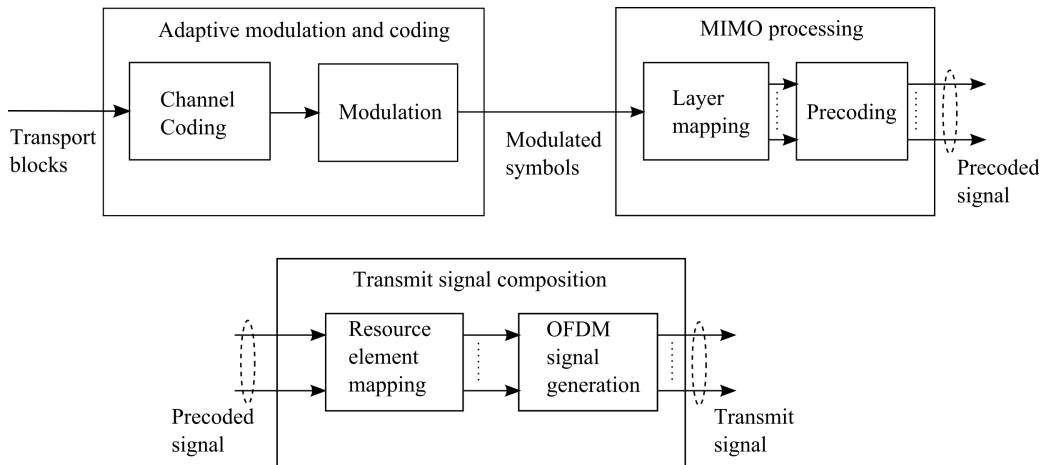

Figure 2.2: LTE physical layer processing [17, 15].

The modulated symbols arrive at the layer mapping unit next, where they are mapped to one or several spatial layers. The number of employed layers is often referred to as the transmission rank. Subsequently, the precoding unit maps the spatial layers to the antenna ports. For linear transceiver architectures considered here, this mapping can be described by a precoding matrix.

LTE-A defines two types of precoding, namely codebook-based precoding and non-codebook-based precoding. They differ in how the precoding matrix is selected by the eNB and made known to the UE. Note that UEs require this information to properly process the received signal and recover the data symbols. In the case of codebook-based precoding, the precoding matrix is selected from a pre-specified codebook. As the codebook is known at both eNB and UE, only the index of the selected matrix needs to be signaled. With non-codebook-based precoding there is no need to signal any precoder matrix information to UEs. The reason for this is the transmission of so-called UE specific reference signals. They are processed

with the same precoding matrix as the user data, thus enabling the UE to estimate the channel including the precoder. In consequence, the eNB can use an arbitrary matrix for precoding.

The last step of physical layer processing is the transmit signal composition. This includes resource element mapping, followed by OFDM signal generation, both performed separately for each antenna port. The resulting baseband signal is then shifted to the desired carrier frequency and transmitted.

2.1.2   Link Adaptation and Scheduling

Rapid variations in transmission link quality, characteristic for mobile communications, require a dynamical adjustment of transmission parameters. In LTE, link adaptation is achieved by means of Adaptive Modulation and Coding (AMC), i.e. by adapting the code rate and modulation scheme to instantaneous channel quality. The higher the code rate and modulation order are, the higher is the transmission data rate but also the Block Error Ratio (BLER). The goal of AMC is to maximize the obtainable throughput while maintaining BLER below a certain threshold, set to 10^{-1} [18].

Since the eNB does not have the necessary channel knowledge, it is dependent on receiving channel feedback from UEs to employ AMC. The UE feedback is calculated in form of the Channel Quality Indicator (CQI). As shown in Table 2.2,

CQI index	Modulation	Code rate	Data rate [bit/symbol]
1	4-QAM	0.08	0.15
2	4-QAM	0.12	0.23
3	4-QAM	0.19	0.38
4	4-QAM	0.30	0.60
5	4-QAM	0.44	0.88
6	4-QAM	0.59	1.18
7	16-QAM	0.37	1.48
8	16-QAM	0.48	1.91
9	16-QAM	0.60	2.41
10	64-QAM	0.46	2.73
11	64-QAM	0.55	3.32
12	64-QAM	0.65	3.90
13	64-QAM	0.75	4.52
14	64-QAM	0.85	5.12
15	64-QAM	0.93	5.55

Table 2.2: LTE modulation alphabets and coding rates [20].

each CQI value specifies a pair of coding rate and modulation scheme. LTE supports fifteen CQIs corresponding to code rates between 0.08 and 0.93, and 4-, 16- and 64-QAM modulations.

The UE feedback should reflect the quality of the transmission link. The post-equalization SINR, as the most suitable quality measure, is used for the CQI calculation. Since the feedback is provided on an RB basis, it is necessary to average the post-equalization SINR over the corresponding REs. This is achieved by means of Mutual Information Effective SINR Mapping (MIESM) which maps multiple SINR values to a single AWGN-equivalent SNR [17]. This hypothetical AWGN SNR would result in the same average spectral efficiency as the original channel, considering the allocated resources. Finally, the AWGN SNR is mapped to CQI so that a BLER lower than 10^{-1} is achieved. In this case the mapping function is linear, according to simulations performed in [19].
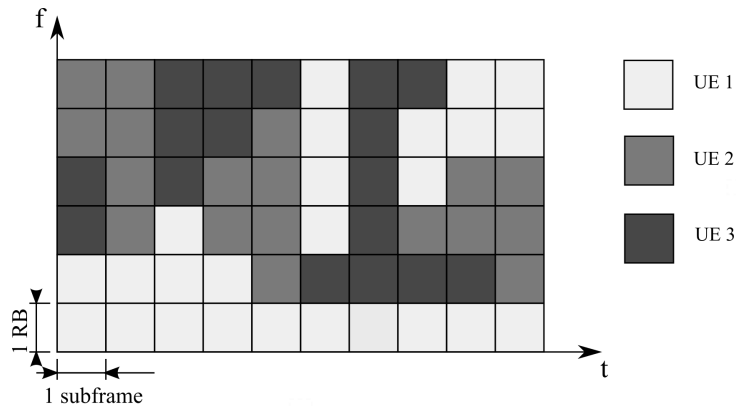

Figure 2.3: LTE time and frequency domain scheduling.

Another way to exploit link quality variations is scheduling. In this case, channel conditions of different UEs are taken into account during resource allocation among them. Scheduling and link adaptation are closely related. They are both performed by the scheduler located on the MAC layer.

Due to the use of OFDM, the LTE scheduler has access to both time and frequency domains. In other words, different RB pairs (two consecutive RBs) can be assigned to different UEs. Figure 2.3 shows an example of resource allocation among three UEs. Similar as for AMC, UEs provide CQI feedback to signalize their channel quality and so support scheduling at the eNB.

LTE standard defines feedback and signaling framework to support scheduling, but it specifies no scheduling algorithms whatsoever. Consequently, there are several scheduling algorithms with different resource allocation strategies [13]. The best CQI scheduler assigns resources to those UEs with the best channel conditions.

Although maximizing the system throughput, this approach cannot guarantee quality of service to all UEs because the ones with bad channel conditions, e.g. cell-edge UEs, are never scheduled. The round robin scheduling provides more fairness among the UEs in a sense that the same amount of resources is assigned to each UE, regardless of the channel conditions. This scheduling approach degrades the system throughput and still doesn't provide the same service quality to all UEs.

A practical scheduler should strike a balance between maximizing the system throughput and maintaining fairness among UEs. An example of such a scheduler is the Proportional Fair (PF) scheduler. The UE chosen by this scheduler has the highest relative channel quality, i.e. the highest instantaneous channel quality relative to its average value. The PF scheduler used in this thesis is described in Section 4.2.1.

2.1.3 CoMP Operation

The term CoMP refers to a wide range of techniques for dynamic coordination between radio communications that is taking place in adjacent cells. The coordination is performed in such a way that the interference between cells is mitigated or even exploited, thereby enhancing the network performance. During the development of LTE-A Release 10, CoMP techniques have been the focus of many 3GPP studies, but weren't standardized until Release 11 [5]. 3GPP adopted CoMP transmission as a tool to improve the coverage of high data rates, and to increase the cell-edge and system throughput. Consequently, a feedback and signaling framework necessary for CoMP operation was defined in LTE-A Release 11.

Downlink CoMP operation requires cooperation among multiple eNBs. The set of eNBs that coordinate their transmissions is defined as the CoMP cooperation set. Typically there are two or three eNBs within one cooperation set. Coordination of more than three eNB is not practical due to the high signaling and processing complexity. The two main types of CoMP cooperation sets are the network predefined and UE-centric cooperation set [10]. In the first case, eNBs are statically divided into sets at the network level. This approach is simple but requires large CoMP cooperation sets. In the case of UE-centric cooperation sets, each UE can determine the set of cooperating eNBs and so supress the ICI more efficiently. The disadvantage of this approach is increased scheduler complexity and signaling overhead. The coordination in the CoMP cooperation set is performed either in centralized manner with a central processing unit, or in distributed manner with eNBs exchanging information over the X2 interface.

The CoMP transmission schemes can basically be classified as Joint Processing (JP), Coordinated Scheduling (CS) and Coordinated Beamforming (CB). With
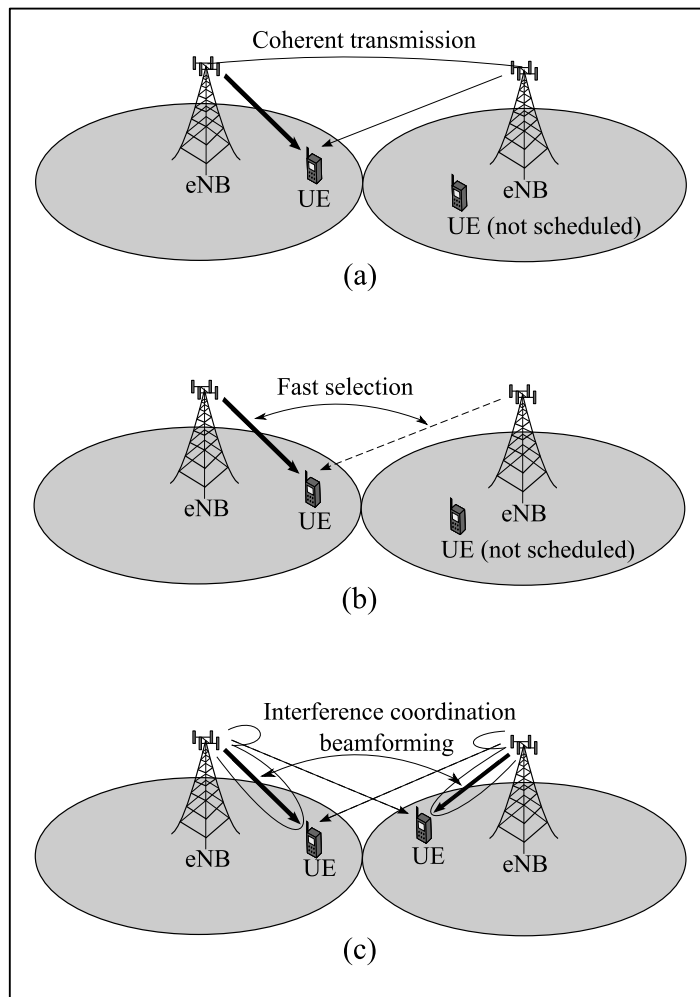
Figure 2.4: CoMP transmission schemes.   (a) Joint Transmission (JT), (b) Dynamic Cell Selection (DCS), and (c) Coordinated Scheduling/Beamforming (CS/CB) [3].

JP, the UE data is available at one cooperating set of eNBs. The data can either be transmitted simultaneously from several eNBs in one RB (Joint Transmission, JT) or be transmitted from one eNB, which can be switched to the best suited eNB within the set for every RB dynamically (Dynamic Cell Selection, DCS). The operating principles of JT and DCS are shown in Figure 2.4 (a) and (b), respectively. JT can be used in combination with DCS, enabling the dynamic selection of multiple transmitting cells.

With CS and CB, the data is only available at one eNB. Within the set, either scheduling decisions (CS) or precoder design (CB) is coordinated to minimize ICI. Figure 2.4 (c) illustrates the principles of CS/ CB. While JP is a more sophisticated CoMP approach, the backhaul requirements are too demanding to be implemented on a commercial scale. Compared with JP, CS and CB require less backhaul overhead and are therefore more suitable for practical implementation.

2.2   System Model

The system considered is a multi-cell network with three cells forming a CoMP cooperation set. Each cell $i \in \{1, 2, 3\}$ in the cooperation set contains an eNB with N_{TX} transmit antennas and J UEs with N_{RX} receive antennas each. The scheduling algorithm selects one UE per cell to be served, leading to a total of three transmitter-receiver pairs on any given time-frequency resource. A model of the resulting interference channel is shown in Figure 2.5.

Both eNB and UE belonging to the cell i are labeled with the same index as the cell, i.e. i. The channel between eNB j and UE i at RE $[n, k]$ is represented by an $N_{RX} \times N_{TX}$ dimensional complex-valued matrix $\mathbf{H}_{i,j}[n, k]$, defined by

$$\mathbf{H}_{i,j}[n, k] = \gamma_{i,j} \tilde{\mathbf{H}}_{i,j}[n, k] \,. \tag{2.2}$$

The parameter $\gamma_{i,j}$ quantitatively describes large-scale path loss, whereas the matrix $\tilde{\mathbf{H}}_{i,j}[n, k]$, whose elements are assumed to have unit variance, characterizes the small-scale fading between eNB j and UE i. Furthermore, it is assumed that channels remain static over the time of scheduling and transmission, and change in i.i.d. fashion across subframes. In this block-fading channel case the time-symbol index n can be dropped.

The symbols to be transmitted from eNB j are compactly written as L dimensional complex symbol vector $\mathbf{s}_j[k]$, where L denotes the number of spatial layers
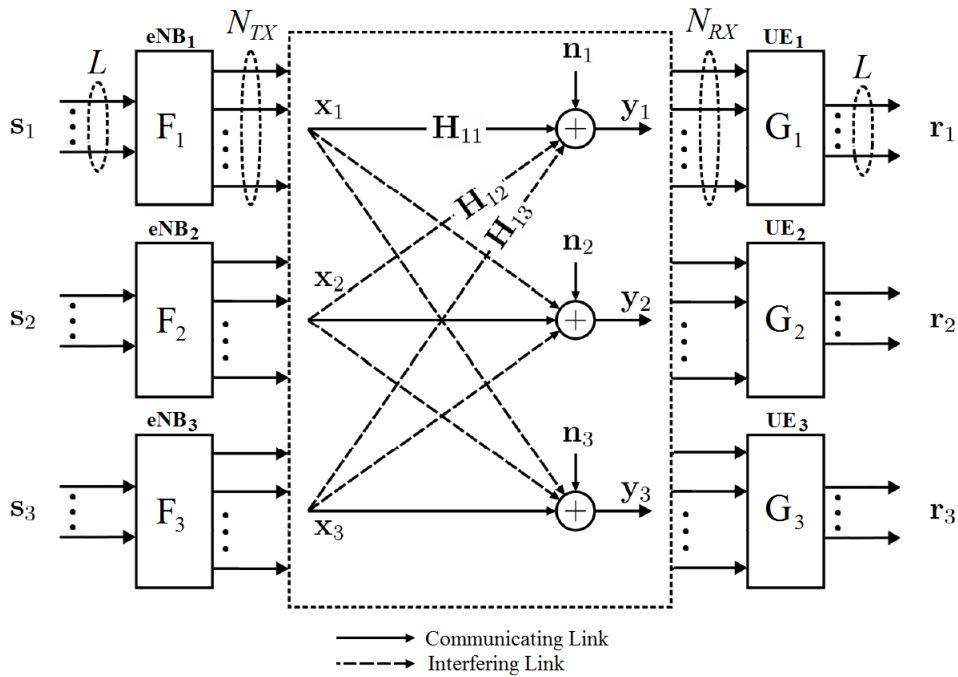

Figure 2.5: Interference channel with three transmitter-receiver pairs.

employed at the eNB and $L \leq L_M = \min(N_{RX}, N_{TX})$. Before transmission, the symbol vector $\mathbf{s}_j[k]$ is multiplied by a precoding matrix $\mathbf{F}_j[k] \in \mathbb{C}^{N_{TX} \times L}$, thus mapping the L symbols to N_{TX} transmit antennas, i.e.

$$\mathbf{x}_j[k] = \mathbf{F}_j[k]\mathbf{s}_j[k] \,, \tag{2.3}$$

where $\mathbf{x}_j[k] \in \mathbb{C}^{N_{TX}}$ constitutes the transmit signal vector at eNB j. The transmit symbol vector and the precoding matrix are normalized as

$$\mathbb{E}\{\mathbf{s}_j[k]\mathbf{s}_j[k]^H\} = \mathbf{I}_L \,, \tag{2.4}$$

$$\mathrm{tr}\left(\mathbf{F}_j[k]\mathbf{F}_j[k]^H\right) = 1 \,. \tag{2.5}$$

Note that equal power allocation among cooperating eNBs and spatial streams is assumed and the transmitted power per UE is normalized to one.

After transmission over the channels, desired and interfering signals as well as the noise add up at each receiver. The signal vector $\mathbf{y}_i[k] \in \mathbb{C}^{N_{RX}}$ received at UE i can therefore be written as

$$\mathbf{y}_i[k] = \mathbf{H}_{i,i}[k]\mathbf{F}_i[k]\mathbf{s}_i[k] + \sum_{\substack{j=1 \\ j \neq i}}^{3} \mathbf{H}_{i,j}[k]\mathbf{F}_j[k]\mathbf{s}_j[k] + \mathbf{n}_i[k] \,, \tag{2.6}$$

where $\mathbf{n}_i[k] \in \mathbb{C}^{N_{RX}}$ denotes the additive white Gaussian noise with distribution $\mathcal{CN}(0, \sigma_n^2 \mathbf{I}_{N_{RX}})$. The first summand in Equation (2.6) is the desired signal at UE i while the second summand represents ICI. Interference from cells outside the CoMP cooperation set is considered a part of the noise. If the number of out-of-set interferers is large, the out-of-set interference is approximately Gaussian distributed due to the central limit theorem.

Given the assumptions above, the average Signal-to-Noise Ratio (SNR) and Signal-to-Interference Ratio (SIR) of UE i are defined as

$$\mathrm{SNR}_i = \frac{\gamma_{i,i}}{\sigma_n^2} \,, \tag{2.7}$$

$$\mathrm{SIR}_i = \frac{\gamma_{i,i}}{\sum_{\substack{j=1 \\ j \neq i}}^{3} \gamma_{i,j}} \,, \tag{2.8}$$

with $\gamma_{i,j}$ being the path loss parameter (see Equation (2.2)).

The received signal $\mathbf{y}_i[k]$ is processed further at UE i, as shown in Figure 2.5. In order to map the N_{RX} streams to L layers an equalizing matrix $\mathbf{G}_i[k]^H \in \mathbb{C}^{L \times N_{RX}}$ is applied, yielding

$$\mathbf{r}_i[k] = \mathbf{G}_i[k]^H \mathbf{y}_i[k] \,, \tag{2.9}$$

or equivalently

$$\mathbf{r}_i[k] = \mathbf{G}_i[k]^H \mathbf{H}_{i,i}[k] \mathbf{F}_i[k] \mathbf{s}_i[k] + \sum_{\substack{j=1 \\ j \neq i}}^{3} \mathbf{G}_i[k]^H \mathbf{H}_{i,j}[k] \mathbf{F}_j[k] \mathbf{s}_j[k] + \mathbf{G}_i[k]^H \mathbf{n}_i[k] \,, \quad (2.10)$$

where $\mathbf{r}_i[k] \in \mathbb{C}^L$ denotes the receive symbol vector, an estimation of the corresponding symbol vector $\mathbf{s}_i[k]$ transmitted from eNB i. It is assumed that each UE is able to perfectly estimate its own channel as well as both of the interference channels and send this information to the serving eNB over a zero-delay error-free feedback channel. The transmitter thus has perfect channel knowledge. In addition, perfect timing and frequency synchronization of UEs and eNBs is assumed.

The symbols originating from different eNBs are assumed statistically independent and also independent of noise. Then the instantaneous post-equalization SINR of UE i, defined for every spatial layer $l \in \{1, 2, \ldots, L\}$, can be computed as

$$\mathrm{SINR}_i^{(l)}[k] = \frac{\left| \mathbf{g}_i^{(l)}[k]^H \mathbf{H}_{i,i}[k] \mathbf{f}_i^{(l)}[k] \right|^2}{\sum_{\substack{p=1 \\ p \neq l}}^{L} \left| \mathbf{g}_i^{(l)}[k]^H \mathbf{H}_{i,i}[k] \mathbf{f}_i^{(p)}[k] \right|^2 + \sum_{\substack{j=1 \\ j \neq i}}^{3} \left\| \mathbf{g}_i^{(l)}[k]^H \mathbf{H}_{i,j}[k] \mathbf{F}_j[k] \right\|^2 + \sigma_n^2 \left\| \mathbf{g}_i^{(l)}[k] \right\|^2} \,,$$
$$(2.11)$$

where $\mathbf{g}_i^{(l)}[k]$ and $\mathbf{f}_i^{(l)}[k]$ denote the l-th column of matrices $\mathbf{G}_i[k]$ and $\mathbf{F}_i[k]$, respectively. The first term in the denominator of Equation (2.11) is the residual interference power between the layers. The second and third term represent the ICI power and the noise power, respectively. Although typically used as performance indicating parameter, SINR can also be employed to design beamforming and scheduling algorithms, as will be shown in Sections 3.1 and 4.1.

Chapter 3

Coordinated Beamforming

3.1 Beamforming Algorithms

The main goal of eNB coordination in CB is to mitigate ICI in order to maximize the throughput of every cell in the CoMP cooperation set. As commonly known, the achievable per-user throughput is upper bounded by Shannon's channel capacity [21]

$$C = \log_2(1 + \text{SINR}).\tag{3.1}$$

A good way to enhance the system throughput is therefore to increase the SINR.

In this chapter, it is assumed that the UE scheduling is already performed, i.e. the set of scheduled UEs is already determined. The focus lies on the CB part where eNBs jointly design transmit beamforming matrices such that the SINR for each UE is maximized. However, this is a complicated optimization problem that involves coupled variables. Several alternative CB strategies have been proposed instead. Some of them focus on canceling ICI perfectly, others aim at minimizing the Mean Squared Error (MSE) of the signal estimation. The three algorithms with different linear precoding strategies are described in the following. To shorten notations, the subcarrier index k is mostly omitted.

3.1.1 ZIOP Algorithm

The Zero Interference by Orthogonal Precoding (ZIOP) algorithm aims at perfectly removing ICI while also maximizing the desired signal power. Similar beamforming schemes, such as block diagonalization [22] and interference alignment [23], focus solely on interference elimination completely ignoring the transmission gain of the desired signal.

The derivation presented in this section is an extension of the one considered in [24] for multiple transmission streams. Assuming that equalizing matrices applied

at every UE are a-priori known at eNB i, the ICI elimination condition can be formulated as

$$
\begin{aligned}
\mathbf{G}_j^H \mathbf{H}_{j,i} \mathbf{F}_i &= \mathbf{0}_{L \times L}\,, \\
\mathbf{G}_m^H \mathbf{H}_{m,i} \mathbf{F}_i &= \mathbf{0}_{L \times L}\,,
\end{aligned}
\tag{3.2}
$$

$\forall i, j, m \in \{1, 2, 3\}$ and $i \neq j \neq m$. By defining the matrix $\mathbf{\Gamma}_i \in \mathbb{C}^{2L \times N_{TX}}$ as

$$
\mathbf{\Gamma}_i = [\mathbf{H}_{j,i}^H \mathbf{G}_j,\ \mathbf{H}_{m,i}^H \mathbf{G}_m]^H\,,
\tag{3.3}
$$

the previously given set of conditions reduces to

$$
\mathbf{\Gamma}_i \mathbf{F}_i = \mathbf{0}_{2L \times L}\,,
\tag{3.4}
$$

implying that $\mathbf{F}_i$ has to lie in the null space of $\mathbf{\Gamma}_i$. Assuming $\mathbf{\Gamma}_i$ is a full rank matrix, the relation between the rank and nullity of $\mathbf{\Gamma}_i$ gives the feasibility condition

$$
N_{TX} \geq 3L\,,
\tag{3.5}
$$

that has to be fulfilled to assure the existence of the solution for $\mathbf{F}_i$. This imposes a restriction on the number of transmit antennas and employed spatial layers.

Provided the feasibility condition is satisfied, the resulting precoding matrix can be written in general form as

$$
\mathbf{F}_i^{\mathrm{ZIOP}} = \alpha_i \mathbf{B}_i \tilde{\mathbf{F}}_i\,,
\tag{3.6}
$$

with $\mathbf{B}_i \in \mathbb{C}^{N_{TX} \times (N_{TX} - 2L)}$ and $\tilde{\mathbf{F}}_i \in \mathbb{C}^{(N_{TX} - 2L) \times L}$. The scaling factor α_i ensures that the power constraint on the precoding matrix, given by Equation (2.5), holds. The matrix $\mathbf{B}_i$ lies in the left null space of $\mathbf{\Gamma_i}$ and $\tilde{\mathbf{F}}_i$ is chosen such that the desired signal power at UE i is maximized. This optimization problem is formulated for every column l of $\tilde{\mathbf{F}}_i$ as

$$
\tilde{\mathbf{f}}_i^{(l)} = \arg\max_{\tilde{\mathbf{f}}} \left| (\mathbf{g}_i^{(l)})^H \mathbf{H}_{i,i} \tilde{\mathbf{f}} \right|^2\,.
\tag{3.7}
$$

In the case of single stream transmission ($L = 1$), the precoding vector of eNB i is given by

$$
\mathbf{f}_i^{\mathrm{ZIOP}} = \alpha_i \left(\mathbf{I}_{N_{TX}} - \hat{\mathbf{\Gamma}}_i^H (\hat{\mathbf{\Gamma}}_i \hat{\mathbf{\Gamma}}_i^H)^{-1} \hat{\mathbf{\Gamma}}_i \right) \mathbf{H}_{i,i}^H \mathbf{g}_i\,,
\tag{3.8}
$$

where $\hat{\mathbf{\Gamma}}_i \in \mathbb{C}^{2 \times N_{TX}}$ can be defined analogous to $\mathbf{\Gamma}_i$ as

$$
\hat{\mathbf{\Gamma}}_i = [\mathbf{H}_{j,i}^H \mathbf{g}_j,\ \mathbf{H}_{m,i}^H \mathbf{g}_m]^H\,.
\tag{3.9}
$$

In order to reduce overhead, the UE feedback is provided on a RB-basis. Consequently, the precoder is calculated only once for all subcarriers k in RB $[\eta, \kappa]$. The

channel matrix observed at the last subcarrier, $\mathbf{H}_{i,j}[12\kappa]$, is chosen as feedback for the ZIOP algorithm.

Since the ICI is precanceled at eNBs, every UE can select its equalizing matrix so that the own channel gain is maximized. For this purpose, the channel between eNB i and UE i is decomposed using the compact-form Singular Value Decomposition (SVD)

$$\mathbf{H}_{i,i} = \mathbf{U}_{i,i}\mathbf{\Sigma}_{i,i}\mathbf{V}_{i,i}^{H}, \tag{3.10}$$

with semi-unitary matrices $\mathbf{U}_{i,i} \in \mathbb{C}^{N_{RX} \times L_M}$ and $\mathbf{V}_{i,i} \in \mathbb{C}^{N_{TX} \times L_M}$ denoting the matrices of left singular vectors and right singular vectors, respectively, and diagonal matrix $\mathbf{\Sigma}_{i,i} \in \mathbb{C}^{L_M \times L_M}$ containing $L_M = \min(N_{RX}, N_{TX})$ singular values of $\mathbf{H}_{i,i}$ in decreasing order. The equalizing matrix at UE i is thus obtained by collecting the first L left singular vectors of $\mathbf{H}_{i,i}$, i.e.

$$\mathbf{G}_i = [\mathbf{u}_{i,i}^{(1)}, \mathbf{u}_{i,i}^{(2)}, \dots \mathbf{u}_{i,i}^{(L)}]. \tag{3.11}$$

3.1.2 LBP Algorithm

The aim of Leakage-Based Precoding (LBP) at the eNB is to maximize the desired signal power at the target UE while minimizing the interference power caused to other co-scheduled UEs. The LBP algorithm is based on the idea in [25], originally proposed for broadcast channels, where the so-called Signal-to-Leakage-plus-Noise Ratio (SLNR) is used as the optimization metric for the precoder design.

When eNB i transmits the signal $\mathbf{x}_i = \mathbf{F}_i\mathbf{s}_i$, the target UE i receives $\mathbf{H}_{i,i}\mathbf{F}_i\mathbf{s}_i$ as the desired component of $\mathbf{y}_i$ (see Equation (2.6)). However, the transmitted signal also reaches other scheduled UEs, causing the total interference of $\sum_{\substack{j=1 \\ j \neq i}}^{3} \mathbf{H}_{j,i}\mathbf{F}_i\mathbf{s}_i$. The SLNR of eNB i, defined as the ratio of the desired signal power at UE i to the interference power caused to other UEs plus noise, can thus be expressed as

$$\text{SLNR}_i = \frac{\mathbb{E}\left\{\mathbf{s}_i^{H}\mathbf{F}_i^{H}\mathbf{H}_{i,i}^{H}\mathbf{H}_{i,i}\mathbf{F}_i\mathbf{s}_i\right\}}{\mathbb{E}\left\{\mathbf{s}_i^{H}\mathbf{F}_i^{H}\sum_{\substack{j=1 \\ j \neq i}}^{3}\mathbf{H}_{j,i}^{H}\mathbf{H}_{j,i}\mathbf{F}_i\mathbf{s}_i\right\} + \mathbb{E}\left\{\mathbf{n}_i^{H}\mathbf{n}_i\right\}}. \tag{3.12}$$

Using Equations (2.4) and (2.5), the expression can be further simplified to

$$\text{SLNR}_i = \frac{\text{tr}\left(\mathbf{F}_i^{H}\mathbf{H}_{i,i}^{H}\mathbf{H}_{i,i}\mathbf{F}_i\right)}{\text{tr}\left(\mathbf{F}_i^{H}\left(\sum_{\substack{j=1 \\ j \neq i}}^{3}\mathbf{H}_{j,i}^{H}\mathbf{H}_{j,i} + N_{RX}\sigma_n^2\mathbf{I}_{N_{TX}}\right)\mathbf{F}_i\right)}. \tag{3.13}$$

The precoder design problem for eNB i is then formulated as

$$\mathbf{F}_i^{\text{LBP}} = \arg\max_{\mathbf{F}_i} \text{SLNR}_i,$$
$$\text{subject to: } \text{tr}\left(\mathbf{F}_i\mathbf{F}_i^{H}\right) = 1. \tag{3.14}$$

Such maximization problem has a closed form solution only for $L = 1$, i.e. single stream transmission [26]. In this case, the SLNR of eNB i is given as

$$\text{SLNR}_i = \frac{\mathbf{f}_i^H \mathbf{H}_{i,i}^H \mathbf{H}_{i,i} \mathbf{f}_i}{\mathbf{f}_i^H \left(\sum_{\substack{j=1 \\ j\neq i}}^3 \mathbf{H}_{j,i}^H \mathbf{H}_{j,i} + N_{RX}\sigma_n^2 \mathbf{I}_{N_{TX}} \right) \mathbf{f}_i} \,. \tag{3.15}$$

Notice that the Equation (3.15) is in the form of a Rayleigh quotient with respect to precoding vector $\mathbf{f}_i$. The solution of the resulting generalized eigenvalue problem is the eigenvector corresponding to the largest eigenvalue of the matrix

$$\mathbf{M}_i = \left(\sum_{\substack{j=1 \\ j\neq i}}^3 \mathbf{H}_{j,i}^H \mathbf{H}_{j,i} + N_{RX}\sigma_n^2 \mathbf{I}_{N_{TX}} \right)^{-1} \mathbf{H}_{i,i}^H \mathbf{H}_{i,i} \,, \tag{3.16}$$

compactly written as

$$\mathbf{f}_i^{\text{LBP}} = \alpha_i \mathbf{v}_{max,1}\{\mathbf{M}_i\} \,. \tag{3.17}$$

with a scaling factor α_i that ensures $\|\mathbf{f}_i\| = 1$.

For the case of multiple spatial streams ($L \geq 2$), the columns of the precoding matrix $\mathbf{F}_i$ are chosen as eigenvectors corresponding to L largest eigenvalues of the matrix $\mathbf{M}_i$, i.e.

$$\mathbf{F}_i^{\text{LBP}} = \alpha_i [\mathbf{v}_{max,1}\{\mathbf{M}_i\}, \mathbf{v}_{max,2}\{\mathbf{M}_i\}, \ldots, \mathbf{v}_{max,L}\{\mathbf{M}_i\}] \,. \tag{3.18}$$

As explained in the previous section, the UE feedback is provided only once per RB. For this purpose, the spatial correlation matrix is utilized [27]. On the RB $[\eta, \kappa]$ and for the channel between eNB i and UE j, it is obtained as

$$\mathbf{R}_{j,i}[\eta, \kappa] = \frac{1}{12} \sum_{k=12\kappa-11}^{12\kappa} \mathbf{H}_{j,i}[k]^H \mathbf{H}_{j,i}[k] \,. \tag{3.19}$$

The precoder at eNB i for all twelve subcarriers $k \in \{12\kappa - 11, 12\kappa - 10, \ldots, 12\kappa\}$ is then calculated with Equation (3.17) for single stream transmission and Equation (3.18) for multiple stream transmission, utilizing the matrix $\mathbf{M}_i$ in modified form, given as

$$\mathbf{M}_i[k] = \left(\sum_{\substack{j=1 \\ j\neq i}}^3 \mathbf{R}_{j,i}[\eta, \kappa] + N_{RX}\sigma_n^2 \mathbf{I}_{N_{TX}} \right)^{-1} \mathbf{R}_{i,i}[\eta, \kappa] \,. \tag{3.20}$$

Clearly, the LBP algorithm does not eliminate ICI. To reduce the impact of the residual interference, a Minimum Mean-Squared Error (MMSE) receiver is employed

at the UEs. The equalizer for UE i is computed to maximize the instantaneous SINR, given by Equation (2.11). The solution can be obtained directly as [13]

$$\mathbf{G}_i = \left(\sum_{j=1}^{3} \mathbf{H}_{i,j} \mathbf{F}_j \mathbf{F}_j^H \mathbf{H}_{j,i}^H + \sigma_n^2 \mathbf{I}_{N_{RX}} \right)^{-1} \mathbf{H}_{i,i} \mathbf{F}_i . \qquad (3.21)$$

3.1.3 Iterative Algorithm

The main objective of this algorithm is to minimize the MSE of the symbol estimation by optimizing both precoder and equalizer. It has been shown, e.g. in [28], that minimizing the MSE is equivalent to maximizing SINR. The following mathematical description is analogous to that shown in [24].

The received symbol vector $\mathbf{r}_i$ at UE i, given by Equation (2.10), is an estimate of the corresponding symbol vector $\mathbf{s}_i$ transmitted from eNB i. The estimation deviation is described by the error vector

$$\mathbf{e}_i = \mathbf{s}_i - \mathbf{r}_i = \mathbf{s}_i - \mathbf{G}_i^H \mathbf{H}_{i,i} \mathbf{F}_i \mathbf{s}_i - \sum_{\substack{j=1 \\ j \neq i}}^{3} \mathbf{G}_i^H \mathbf{H}_{i,j} \mathbf{F}_j \mathbf{s}_j - \mathbf{G}_i^H \mathbf{n}_i . \qquad (3.22)$$

The MSE of the estimation is formulated as

$$\mathrm{MSE}_i = \mathbb{E}\{ \mathrm{tr} \left(\mathbf{e}_i \mathbf{e}_i^H \right) \} , \qquad (3.23)$$

and with the assumptions introduced in Section 2.2, it can be reformulated to

$$\mathrm{MSE}_i = \mathrm{tr}\left(\left(\mathbf{I}_L - \mathbf{G}_i^H \mathbf{H}_{i,i} \mathbf{F}_i \right) \left(\mathbf{I}_L - \mathbf{F}_i^H \mathbf{H}_{i,i}^H \mathbf{G}_i \right) + \sum_{\substack{j=1 \\ j \neq i}}^{3} \mathbf{G}_i^H \mathbf{H}_{i,j} \mathbf{F}_j \mathbf{F}_j^H \mathbf{H}_{i,j}^H \mathbf{G}_i + \sigma_n^2 \mathbf{G}_i^H \mathbf{G}_i \right) .$$
$$(3.24)$$

The design problem can then be stated as

$$\{ \mathbf{G}_i^{\mathrm{Iter}}, \mathbf{F}_i^{\mathrm{Iter}} \} = \arg \min_{\mathbf{G}_i, \mathbf{F}_i} \mathrm{MSE}_i ,$$
$$\text{subject to: } \mathrm{tr} \left(\mathbf{F}_i \mathbf{F}_i^H \right) = 1 , \qquad (3.25)$$

or equivalently as

$$\{ \mathbf{G}_i^{\mathrm{Iter}}, \mathbf{F}_i^{\mathrm{Iter}} \} = \arg \min_{\mathbf{G}_i, \mathbf{F}_i} \left(\mathrm{MSE}_i + \lambda_i \left(\mathrm{tr} \left(\mathbf{F}_i \mathbf{F}_i^H \right) - 1 \right) \right) , \qquad (3.26)$$

where $\lambda_i \geq 0$ is the Lagrange multiplier that ensures a power constraint on precoding vector $\mathbf{F}_i$, i.e. that it is maximally unitary.

Differentiating the expression in Equation (3.26) with respect to $\mathbf{G}_i$ and $\mathbf{F}_i$, and using the Karush-Kuhn-Tucker conditions [29], the following expressions for $\mathbf{G}_i$ and

$\mathbf{F}_i$ are obtained

$$\mathbf{G}_i = \left(\sum_{j=1}^{3} \mathbf{H}_{i,j}\mathbf{F}_j\mathbf{F}_j^H\mathbf{H}_{i,j}^H + \sigma_n^2\mathbf{I}_{N_{RX}}\right)^{-1}\mathbf{H}_{i,i}\mathbf{F}_i, \tag{3.27}$$

$$\mathbf{F}_i = \left(\mathbf{H}_{i,i}^H\mathbf{G}_i\mathbf{G}_i^H\mathbf{H}_{i,i} + \lambda_i\mathbf{I}_{N_{TX}}\right)^{-1}\mathbf{H}_{i,i}^H\mathbf{G}_i. \tag{3.28}$$

Since both equations depend on each other, the equalizer and the precoder must be calculated iteratively. As the starting point, the equalizing matrix given by Equation (3.11) is utilized. Subsequently, both $\mathbf{G}_i$ and $\mathbf{F}_i$ are sequentially updated using Equations (3.27) and (3.28), respectively. Note that the Lagrange multiplier λ_i must be recalculated at each iteration, e.g. by Newton's method [29].

In the case of single stream transmission ($L = 1$), Equations (3.27) and (3.28) can be reformulated using the matrix inversion lemma [29]. They are thus given as [28]

$$\mathbf{g}_i = \left(\sum_{\substack{j=1 \\ j\neq i}}^{3} \mathbf{H}_{i,j}\mathbf{f}_j\mathbf{f}_j^H\mathbf{H}_{i,j}^H + \sigma_n^2\mathbf{I}_{N_{RX}}\right)^{-1}\mathbf{H}_{i,i}\mathbf{f}_i, \tag{3.29}$$

$$\mathbf{f}_i = \frac{\mathbf{H}_{i,i}^H\mathbf{g}_i}{\lambda_i + \mathbf{g}_i^H\mathbf{H}_{i,i}\mathbf{H}_{i,i}^H\mathbf{g}_i}. \tag{3.30}$$

The last equation simply states that $\mathbf{f}_i \sim \mathbf{H}_{i,i}^H\mathbf{g}_i$. Therefore, the Iterative algorithm simplifies to

$$\mathbf{g}_i = \left(\sum_{\substack{j=1 \\ j\neq i}}^{3} \mathbf{H}_{i,j}\frac{\mathbf{H}_{i,i}^H\mathbf{g}_i\mathbf{g}_i^H\mathbf{H}_{i,i}}{\mathbf{g}_i^H\mathbf{H}_{i,i}\mathbf{H}_{i,i}^H\mathbf{g}_i}\mathbf{H}_{i,j}^H + \sigma_n^2\mathbf{I}_{N_{RX}}\right)^{-1}\mathbf{H}_{i,i}\mathbf{f}_i, \tag{3.31}$$

$$\mathbf{f}_i = \frac{\mathbf{H}_{i,i}^H\mathbf{g}_i}{\left\|\mathbf{H}_{i,i}^H\mathbf{g}_i\right\|}. \tag{3.32}$$

Regarding feedback, the channel matrix observed at the last subcarrier of RB $[\eta, \kappa]$ ($\mathbf{H}_{i,j}[12\kappa]$) is fed back by the UE. Consequently, the same precoder and equalizer are employed for all twelve subcarriers $k \in \{12\kappa - 11, 12\kappa - 10, \ldots, 12\kappa\}$.

3.2   Performance Evaluation

The performance of the presented algorithms is assessed by means of extensive link level simulations. In the following sections, the simulation setup and the applied metrics are described. Further, the simulation results are presented and discussed.

3.2.1   Methodology

A network consisting of three cells is considered. Every cell contains five active UEs accommodated by one eNB with four uncorrelated transmit antennas. Simulations for two and four receive antennas at UEs are conducted. Prior to transmission, a set of served UEs is determined by means of Proportional Fair (PF) scheduling. The employed PF scheduler is described in Section 4.2.1. The carrier frequency 2.1 GHz, with a total bandwidth of 1.4 MHz (six RBs) is assumed. For propagation, two channel models, namely frequency-flat Rayleigh and frequency-selective typical urban [30] are used. The transmission rank is restricted to one (single stream transmission). The simulation parameters are summarized in Table 3.1.

Parameter	Value
Carrier frequency	2.1 GHz
System bandwidth	1.4 MHz
Channel models	Flat Rayleigh, 3GPP Typical urban [30]
Channel estimation	Perfect channel knowledge
Number UEs of per cell (J)	5
Antenna configurations ($N_{TX} \times N_{RX}$)	4×2, 4×4
Antenna correlation	Zero correlation
Transmission rank (L)	1
Scheduling algorithm	PF

Table 3.1: Main simulation parameters.

Two different simulation scenarios are employed:

- **CSB Scenario**: The average path loss parameter $\gamma_{i,i}$ between eNB i and UE i is set to one. All other parameters $\gamma_{i,j}$ between eNB j and UE i, and receiver noise variance σ_n^2 are globally defined. As a consequence, the average SNR (Equation (2.7)) and average SIR (Equation (2.8)) are the same for every UE.

- **3BS Scenario**: The UEs are uniformly distributed within $60°$ sectors of three hexagonal cells with 500 m radius. The SIR and SNR are determined by the path loss model, individually for every UE. Shadow fading is not considered. The network layout parameters are listed in Table 3.2.

As a reference design for downlink transmission, a non-CoMP scheme based on SVD is also simulated. This scheme aims to maximize the channel gain between the UE and its serving eNB while treating ICI as additional noise. Therefore, the precoding matrix $\mathbf{F}_i$ applied at eNB i consists of the first L right singular vectors $\mathbf{v}_{i,i}^{(l)}$ of the channel matrix $\mathbf{H}_{i,i}$ (see Equation (3.10)), i.e.

$$\mathbf{F}_i^{\text{Non-CoMP}} = [\mathbf{v}_{i,i}^{(1)}, \mathbf{v}_{i,i}^{(2)}, \dots \mathbf{v}_{i,i}^{(L)}].$$

(3.33)

Parameter	Value
Cell layout	Hexagonal grid, 3 cells with 60° sectors
Cell radius (r_c)	500 m
UE distribution	Uniform
Distance-dependent path loss	$128.1 + 37.6 \log_{10}(d)$ dB, d in kilometers

Table 3.2: Network layout parameters.

The equalizing matrix $\mathbf{G}_i$ used by UE i contains the first L left singular vectors of $\mathbf{H}_{i,i}$ and is given by Equation (3.11). It is easy to show that both LBP and Iterative algorithm reduce to this scheme if the ICI is negligible compared to noise.

The performance of the system is characterized by the UE throughput, cell throughput and Area Spectral Efficiency (ASE) [31], averaged over multiple sub-frames (300 in the CSB scenario and 100 in the 3BS scenario). The UE throughput is referred to as the number of information bits inside a correctly received subframe. The cell throughput is the sum of all UE throughputs in a given cell.

The ASE is used as a metric for the overall network efficiency. In [32], it is estimated as

$$\text{ASE} \approx \frac{1}{r_c^2 \pi} \sum_{m=1}^{M} \tilde{T}_{UE}(r_m) \left(U \frac{r_m^2 - r_{m-1}^2}{r_c^2} \right) , \tag{3.34}$$

where r_c is the cell radius, $\tilde{T}_{UE}(r_m)$ denotes the average UE throughput at a distance from the serving eNB between r_m and r_{m-1}, and U is the total number of UEs in all three cells. For estimation, the cell area is thus split into M rings. For every ring, the average UE throughput is multiplied by the expected number of UEs in this area, given in Equation (3.34) by the term in brackets. The sum is then calculated over all M rings. The value of $\tilde{T}_{UE}(r_m)$ is estimated from 1200 random positions per user. As the radius increment, $\Delta r = r_m - r_{m-1} = 10\,\text{m}$ is used.

3.2.2 Results and Discussion

The simulation results obtained with the CSB scenario are presented in Figures 3.1-3.6, including the 95% confidence intervals. Note that the y-scaling varies among plots.

The first set of simulations evaluates the performance of the algorithms for different channel models and antenna configurations. An SNR of 100 dB is used to make noise negligible and set the focus on the ability to remove interference. Note that the maximal achievable throughput is restricted to about 5.05 Mbit/s, due to the finite set of code rates and finite transport block lengths supported by LTE.
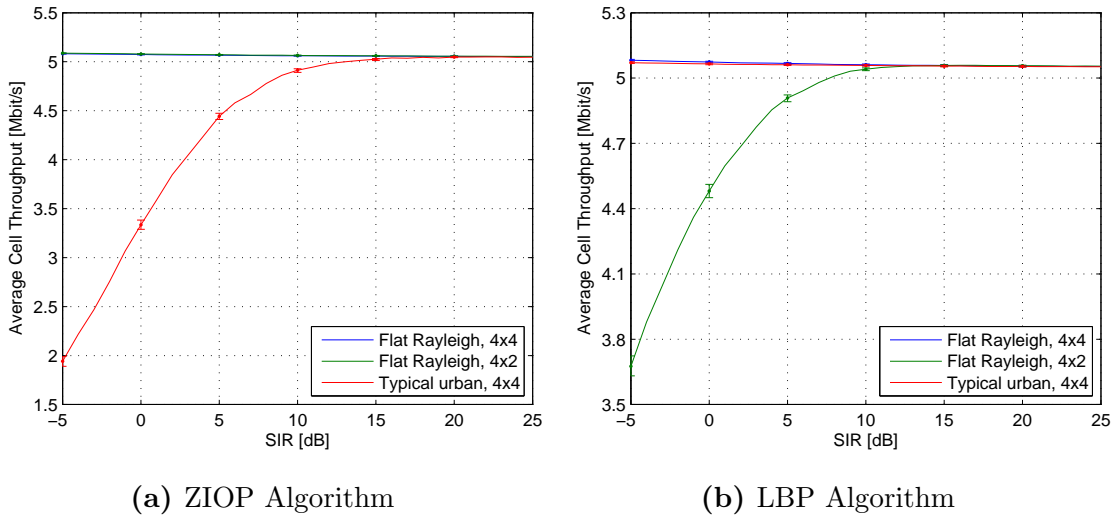
(a) ZIOP Algorithm
(b) LBP Algorithm

Figure 3.1: Average cell throughput over SIR for different channels and antenna setups at SNR = 100 dB.

Figure 3.1 (a) shows the average cell throughput achieved with the ZIOP algorithm. For flat Rayleigh channels, ZIOP is able to completely remove ICI. Because the interference is precanceled at the eNB, the performance is not affected by the number of receive antennas. In typical urban environment, a mismatch between the channel feedback received during precoder calculation and the channel for which the precoder is employed occurs, due to the fact that the precoder is calculated only once per RB. The algorithm is therefore incapable of canceling all ICI, causing the throughput drop in the low SIR region.

The performance of the LBP algorithm is illustrated in Figure 3.1 (b). The spatial correlation matrix, used as feedback for LBP, reflects channel variations. This scheme is thus robust to channel changes and reaches the highest possible throughput in typical urban channels. However, in the case of two receive antennas a strong performance degradation is observed. This is mainly due to the inability of the MMSE receiver to remove the residual interference. In the case of two receive antennas there is a possibility to completely suppress only one interferer.

In Figure 3.2 (a), different number of iterations N_I for the Iterative algorithm are considered for a flat Rayleigh channel with the 4×4 antenna configuration. It can be seen that the algorithm converges as the number of iterations increases. For cost/benefit reasons, N_I equal to 10 is chosen for all further evaluations.

As shown in Figure 3.2 (b), the Iterative algorithm performs best in the case of frequency-flat channel and four receive antennas. As the channel feedback is obtained in the same way as for ZIOP, the same effect of throughput reduction as in Figure 3.1 (a) is observed for typical urban channels. Furthermore, the ICI
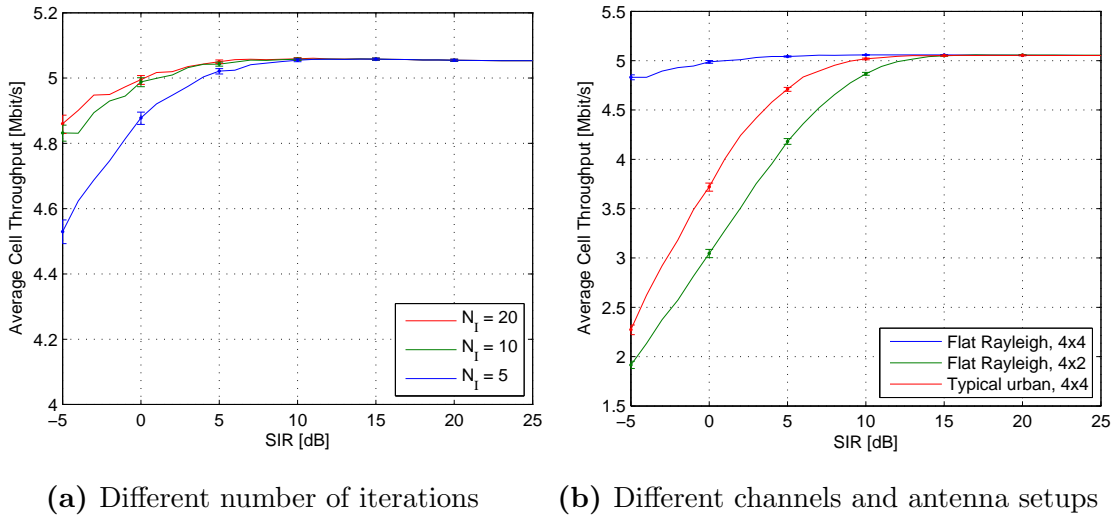
(a) Different number of iterations

(b) Different channels and antenna setups

Figure 3.2: Average cell throughput over SIR for the Iterative algorithm at SNR = 100 dB

removal is performed by the receiver, so the reduction of the receive antennas has the same impact on the performance as for the LBP algorithm.

In Figures 3.3 (a) and (b), the algorithms are compared to each other and to the Non-CoMP scheme in case of the flat Rayleigh fading channel. It can be seen that all CB schemes significantly outperform the Non-CoMP scheme, especially in the low SIR region. This is attributed to the fact that this scheme treats the interference as an additional noise and does not try to reduce it. Notice that the performance
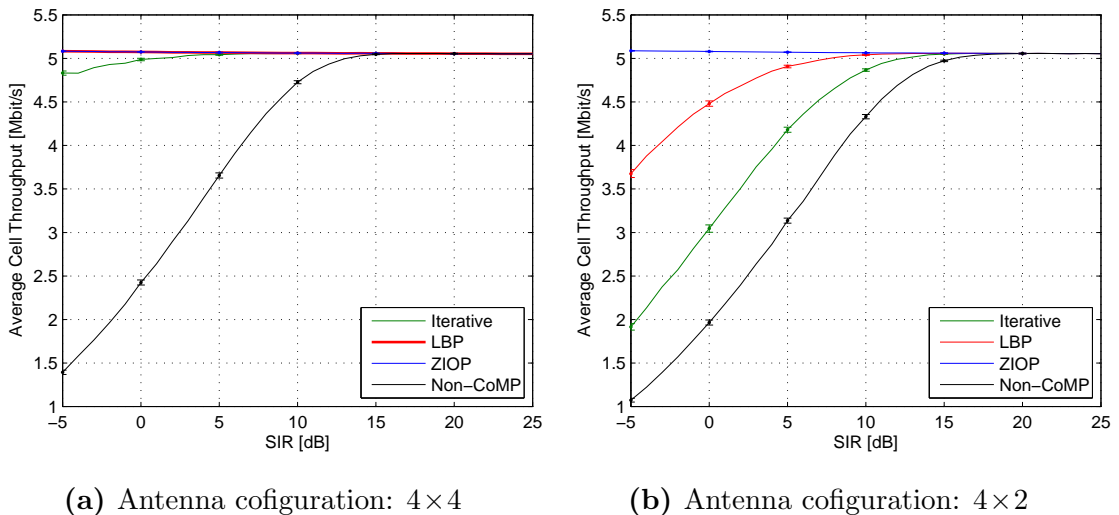

(a) Antenna cofiguration: 4×4

(b) Antenna cofiguration: 4×2

Figure 3.3: Average cell throughput over SIR for different beamforming algorithms and flat Rayleigh channel at SNR = 100 dB
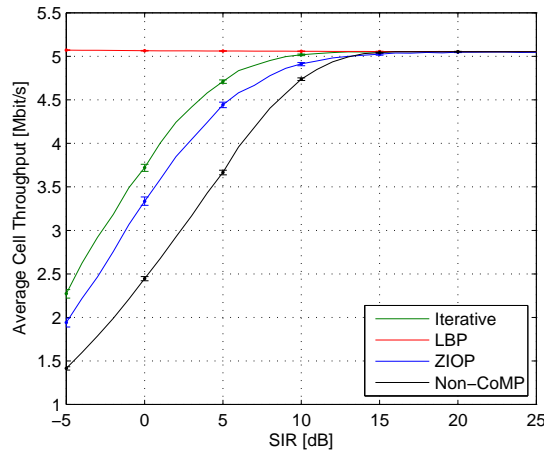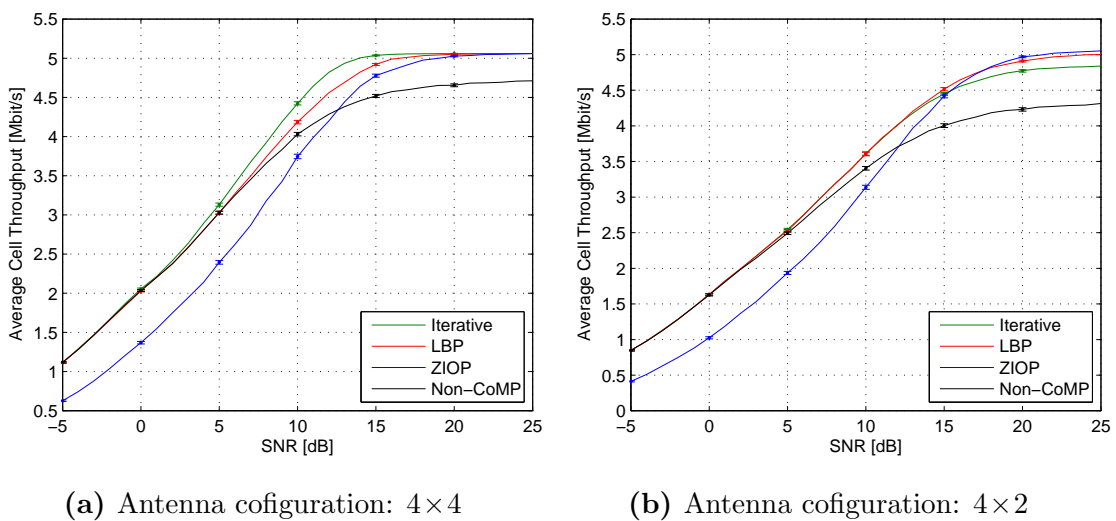
Figure 3.4: Average cell throughput over SIR for different beamforming algorithms and typical urban channel at SNR = 100 dB

loss of the Iterative algorithm in the two receive antenna case is significantly higher than that of the LBP algorithm. Unlike LBP, the precoder for the Iterative scheme is calculated only to maximize the channel gain, no interference considered.

Figure 3.4 shows the algorithm comparison for the typical urban channel and 4×4 antenna configuration. The Non-CoMP scheme is here also outperformed by the CB schemes. However, the performance improvement of the ZIOP and Iterative algorithm is smaller than in the flat Rayleigh case.

The next set of simulations investigates the behavior of the algorithms in dependance of the noise level. For these simulations, the SIR value is set to 10dB to

(a) Antenna cofiguration: 4×4

(b) Antenna cofiguration: 4×2

Figure 3.5: Average cell throughput over SNR for different beamforming algorithms and flat Rayleigh channel at SIR = 10 dB
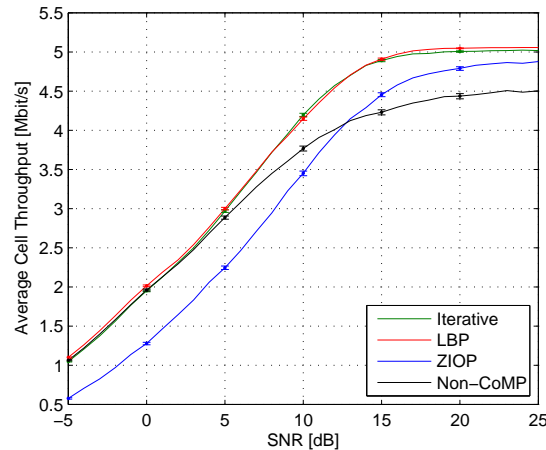
Figure 3.6: Average cell throughput over SNR for different beamforming algorithms and typical urban channel at SIR = 10 dB

reflect a realistic amount of interference.

In Figure 3.5, the algorithms are compared for the flat Rayleigh channel case. Both plots show ZIOP under-performing in regions where the SNR is lower than the SIR, since ZIOP is primarily focused on eliminating ICI. As soon as the SNR is significantly higher than the SIR (at about 13dB), ZIOP gains in throughput, outperforming the Non-CoMP scheme. Additionally, when 2 receive antennas are employed, it also outperforms the LBP and the Iterative scheme at high SNR. It can be seen that in the low SNR region, Iterative, LBP and Non-CoMP achieve the same throughput. As explained in Section 3.2.1, the precoders and equalizers are equivalent to each other in this case. Similar effects can be observed in Figure 3.6 for the typical urban channel model.

The simulation results obtained with the 3BS scenario are presented in the following. In this scenario, the UEs are uniformly distributed over the 60° sectors. The throughput distribution within the sector can be depicted by an Empirical Cumulative Distribution Function (ECDF). For all simulations, the flat Rayleigh channel model is used.

In Figure 3.7 (a) and (b), the distribution of the average cell throughput for the four and two transmit antenna case, respectively, is illustrated. The ZIOP algorithm performs worst in both cases, due to the relatively high noise level caused mainly by the interference from outside of the CoMP cooperation set. The LBP and the Iterative algorithm both outperform the Non-CoMP scheme. When four antennas are employed by the eNBs, the Iterative algorithm achieves the highest throughput. However, if the number of receive antennas is reduced to two, this scheme is outperformed by the LBP algorithm.
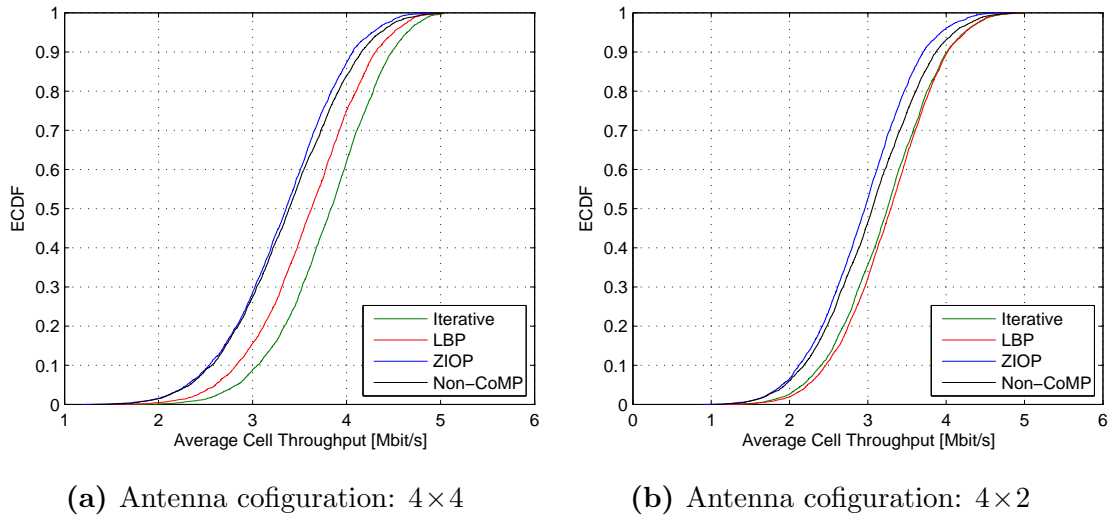
(a) Antenna cofiguration: 4×4 **(b)** Antenna cofiguration: 4×2

Figure 3.7: Cell throughput distributions of different beamforming algorithms

The next simulations show the influence the different algorithms have on the average UE throughputs. In Figure 3.8, the bottom 5% of the ECDF depict the cell-edge throughput. ZIOP performs worse than all other schemes at cell-edge, as well as near the eNB. However, within the cell there are regions where ZIOP has an advantage over the Non-CoMP scheme. In similar regions, LBP outperforms the Iterative scheme in a 4×2 antenna configuration, while the Iterative algorithm provides the best performance in the 4×4 antenna setup.

In Figure 3.9 (a), the average throughput is used as an overall system performance measure, while Figure 3.9 (b) shows the cell-edge throughput. Compared
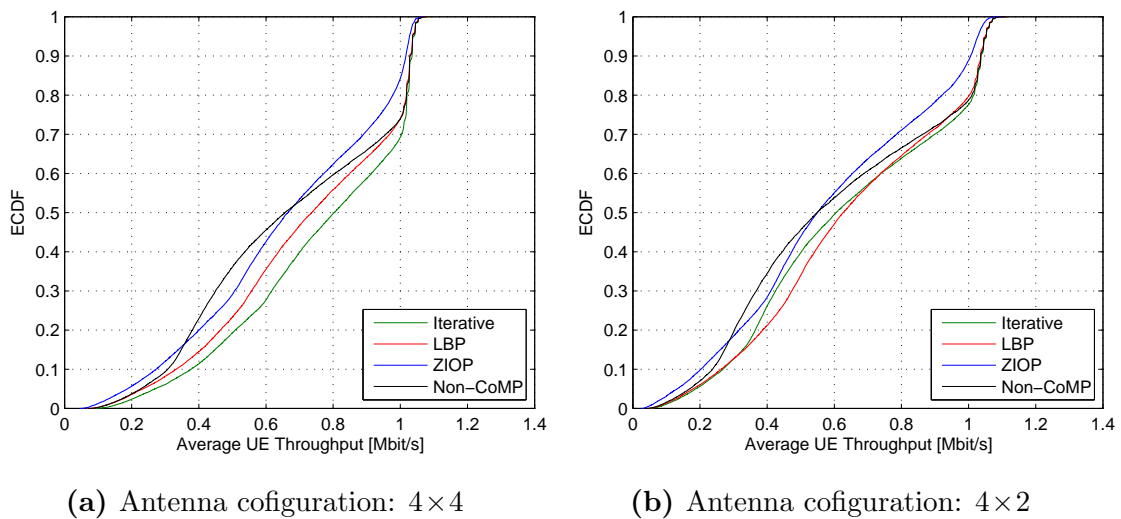

(a) Antenna cofiguration: 4×4 **(b)** Antenna cofiguration: 4×2

Figure 3.8: UE throughput distributions of different beamforming algorithms

(a) Mean value

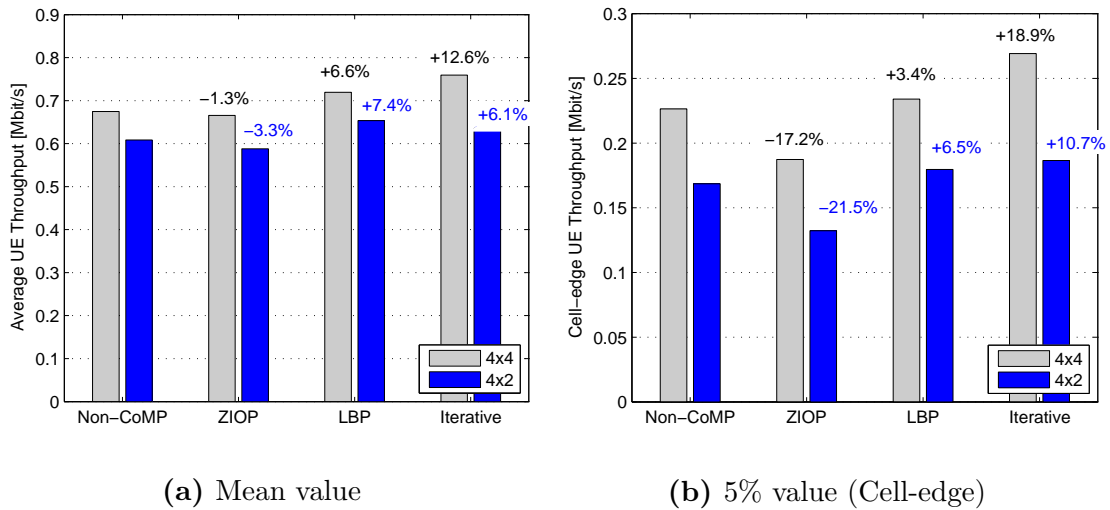**(b)** 5% value (Cell-edge)

Figure 3.9: UE throughput of different beamforming algorithms

to Non-CoMP, ZIOP provides slightly lower average throughput $(-1\%, -3\%)$, but performs significantly worse $(-17\%, -22\%)$ at the cell-edge. LBP on the contrary gains both in average $(6\%, 7\%)$ and cell-edge throughput $(3\%, 6\%)$. The iterative algorithm outperforms Non-CoMP on average by 13% for 4×4 and 6% for 4×2 antennas, also on the cell edge with 19% and 11% respectively. Note the difference in the achieved UE throughput between 2 and 4 receive antennas.

Figure 3.10 depicts the Area Spectral Efficiency (ASE) of the algorithms. Compared to Non-CoMP, all algorithms achieve a higher ASE. ZIOP has minimal advantage, with only $+4\%, +2\%$.While it might seem counterintuitive that ZIOP has a higher ASE than Non-CoMP while performing worse in Figure 3.9, this is due to the fact that in a significant portion of the cell, ZIOP outperforms Non-CoMP as can be seen in Figure 3.8. LBP utilizes the 4×2 configuration most efficiently with $+14\%$, the Iterative scheme gains most in the 4x4 configuration $(+19\%)$.
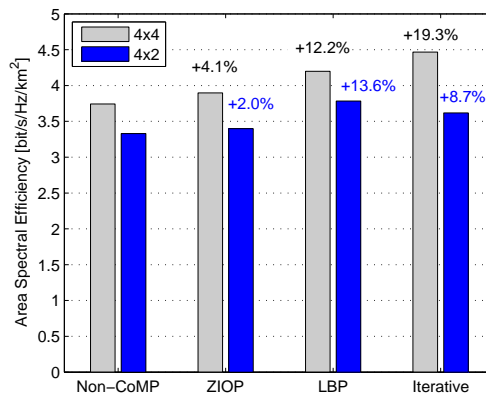

Figure 3.10: ASE of different beamforming algorithms

27

Chapter 4

Coordinated Scheduling

4.1 Scheduling Algorithm

The scheduler attempts to optimally allocate resources among UEs in the time and frequency domain, so that the system throughput is as high as possible. With ICI being a considerable obstacle in this context, eNBs have to cooperate in their scheduling processes to effectively prevent interference, thus employing the concept of CS. With CS, eNBs gather channel feedback from UEs located in the CoMP cooperation set and schedule UE groups according to their summed throughput.

With channel feedback being provided in RB granularity, scheduling is done on an RB-basis. The i-th set of UEs considered for scheduling in RB $[\eta, \kappa]$ is denoted as $\mathcal{S}_i[\eta, \kappa]$. The presented algorithm is based on exhaustive search employing the achievable sum rate, that is defined for UE set $\mathcal{S}_i[\eta, \kappa]$ as

$$C_{\mathcal{S}_i}[\eta, \kappa] = \sum_{s \in \mathcal{S}_i} \sum_{k=12\kappa-11}^{12\kappa} \sum_{l=1}^{L} \log_2(1 + \mathrm{SINR}_s^{(l)}[k]), \qquad (4.1)$$

where $\mathrm{SINR}_s^{(l)}$ is the instantaneous SINR for UE s, given by Equation (2.11). Thereby, it is assumed that eNBs are going to calculate their precoders with LBP algorithm and UEs will employ MMSE receivers. The scheduling scheme is therefore called Leakage-Based (LB) scheduling. It is built upon the algorithms presented in [27, 33].

The LB scheduling steps are described below. As the procedure is the same for every RB, the corresponding indices η and κ are omitted.

1. Build all possible sets (J^3) consisting of one UE from each cell in the CoMP cooperation set, respectively. The i-th UE set $\mathcal{S}_i$ contains three elements $s_1, s_2, s_3 \in \{1, 2, \ldots, J\}$ where UE s_1 belongs to the first cell, UE s_2 to the second and UE s_3 to the third cell. Gather feedback in form of spatial correlation matrices (Equation (3.19)) for all involved UEs.

Repeat the steps 2. and 3. for all $i \in \{1, 2, \ldots, J^3\}$.

2. Compute precoding and equalizing matrices for all UEs in $\mathcal{S}_i$ using LBP and MMSE equalization, respectively. The corresponding expressions are derived in Section 3.1.2 and are given by Equations (3.18) and (3.21).

3. Calculate the achievable sum rate of $\mathcal{S}_i$ using the Equation (4.1).

4. Select the UE set with the highest achievable sum rate $C_{\mathcal{S}}$.

Notice that the required computational effort grows cubically with J. This is feasible only for a small number of UEs per cell. Otherwise, a limited number of UEs should be preselected to reduce complexity. The UE preselection in a cell can be done e.g. based on the proportional fairness metric [34].

4.2   Performance Evaluation

In this section, link level simulations are used to asses the performance of the presented algorithm. A brief description of the simulation setup is followed by simulation results and discussion.

4.2.1   Methodology

In the following simulations, LB and PF scheduling are compared. The simulation setup is basically the same as in Section 3.2.1, with the exception that the LBP algorithm is applied at the eNBs and MMSE receivers at the UEs. The simulation parameters are summarized in Table 4.1.

Parameter	Value
Carrier frequency	2.1 GHz
System bandwidth	1.4 MHz
Channel models	Flat Rayleigh, 3GPP Typical urban [30]
Channel estimation	Perfect channel knowledge
Number UEs of per cell (J)	5
Antenna configurations ($N_{TX} \times N_{RX}$)	4×2, 4×4
Antenna correlation	Zero correlation
Transmission rank (L)	1
Precoding algorithm	LBP
Receiver algorithm	MMSE

Table 4.1: Main simulation parameters.

The PF scheduling, which is utilized here as the benchmark for comparison, does not allow for cell coordination. The decision which UE is served on a given RB is therefore made independently in each cell. In order to ensure fair resource allocation, the scheduling decision is based on the metric defined for UE j as

$$\mathcal{R}_j[\eta, \kappa] = \frac{C_j[\eta, \kappa]}{\bar{T}_j[\eta]} \,, \tag{4.2}$$

where C_j is computed by Equation (4.1), with the UE set containing only UE j, and $\bar{T}_j$ denotes the UE throughput averaged over t_c slots. This throughput value is computed recursively, using an exponentially weighted low-pass filter [34]

$$\bar{T}_j[\eta] = \begin{cases} \left(1 - \frac{1}{t_c}\right) \bar{T}_j[\eta - 1] + \frac{1}{t_c} C_j[\eta - 1] & \text{if UE } j \text{ scheduled at } \eta - 1\,, \\ \left(1 - \frac{1}{t_c}\right) \bar{T}_j[\eta - 1] & \text{if UE } j \text{ not scheduled at } \eta - 1\,. \end{cases} \tag{4.3}$$

At any scheduling instant, the UE with the highest weighted rate $\mathcal{R}$ is chosen for transmission. The parameter t_c is set to 10.

The performance of a scheduler is not solely characterized by the achieved throughput, the fairness in the resource allocation has to be considered as well. Jain's Fairness Index (JFI) [35] is used as a metric for fairness comparison. It is computed as

$$\text{JFI} = \frac{\left(\sum_{j=1}^{J} \tilde{T}_j\right)^2}{J \sum_{j=1}^{J} \tilde{T}_j^2} \,, \tag{4.4}$$

where $\tilde{T}_j$ is the average throughput of UE j. The value of JFI ranges from $\frac{1}{J}$, when one UE gets all resources, to 1, when the achieved throughputs of all UEs are the same and perfect fairness is achieved.

4.2.2 Results and Discussion

The results obtained with the CSB simulation scenario are presented first, including the 95% confidence intervals. Note that the y-scaling varies from plot to plot.

Figure 4.1 evaluates LB scheduling for different channel models and antenna configurations. For two receive antennas, a drop in cell throughput occurs with decreasing SIR. This is due to the employed MMSE receiver. The same effect can be seen in Figure 3.1 (b) and was already accounted for in Section 3.2.2. In case of the frequency selective channel, the maximal achievable throughput is slightly lower than in the flat Rayleigh case. This happens because the algorithm schedules several UEs in TTI, resulting in shorter transport blocks compared to the frequency-flat case where the same UE is always scheduled. Thereby, the system overhead increases, reducing the useful information transmitted.
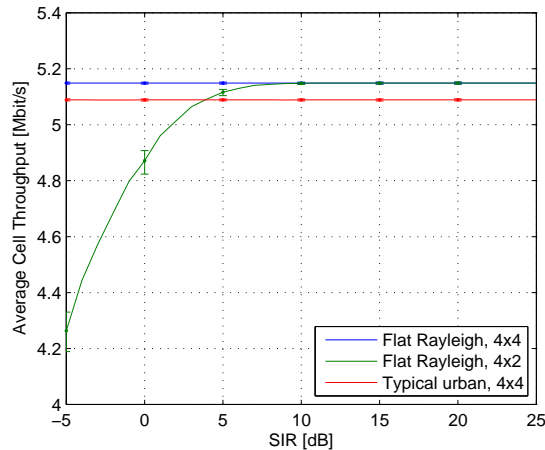
Figure 4.1: Average cell throughput over SIR for the LB scheduling algorithm at SNR = 100 dB

In Figure 4.2, the performance of the LB scheduler is compared to that of the PF scheduler for typical urban channel and 4×2 antenna configuration. In the low SIR region, LB scheduling provides a persistent throughput gain over PF scheduling. With increasing SIR, a similar effect to the one discussed for Figure 4.1 becomes apparent, because the PF algorithm also schedules different UEs per TTI.

Figure 4.3 shows the average cell throughput as a function of SNR for the two scheduling algorithms. In both low and high SNR regions, a similar behavior as in Figure 4.2 can be observed. The schedulers select UEs based on the achievable sum rate (Equation (4.1)), making them equally susceptible to both SNR and SIR.
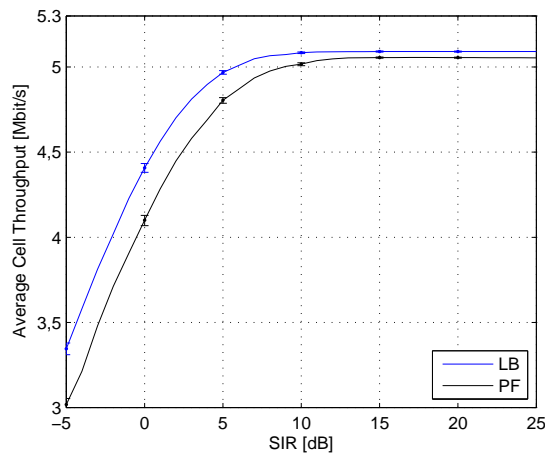

Figure 4.2: Average cell throughput over SIR for different scheduling algorithms and typical urban channel at SNR = 100 dB
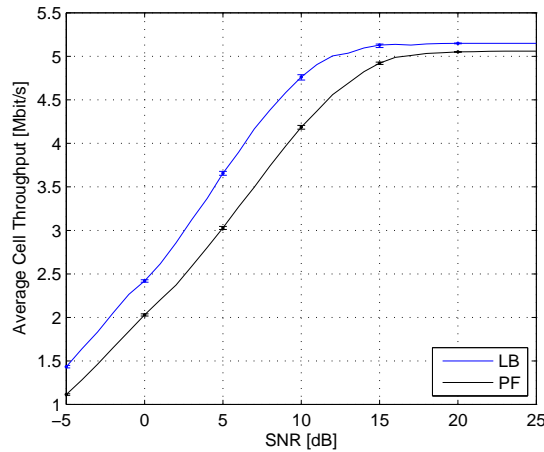
Figure 4.3: Average cell throughput over SNR for different scheduling algorithms and flat Rayleigh channel at SIR = 10 dB

The simulation results obtained with the 3BS scenario are presented next. All simulations are conducted using the flat Rayleigh channel model.

The ECDF of the average cell throughput for LB and PF scheduling with a 4x4 antenna setup is depicted in Figure 4.4. As already illustrated in Figures 4.2 and 4.3, the LB scheme clearly outperforms the PF scheme. It is extremely likely that a high cell throughput is achieved by the LB scheduler.

The average and cell-edge UE throughputs are illustrated in Figure 4.5 (a) and (b), respectively. Like in Figure 4.4, LB scheduling is more than tripling average UE throughput. However, Figure 4.5 (b) shows that UEs at the cell-edge are penalized by the LB scheduler to nearly a fifth of the throughput compared to the PF scheduler.
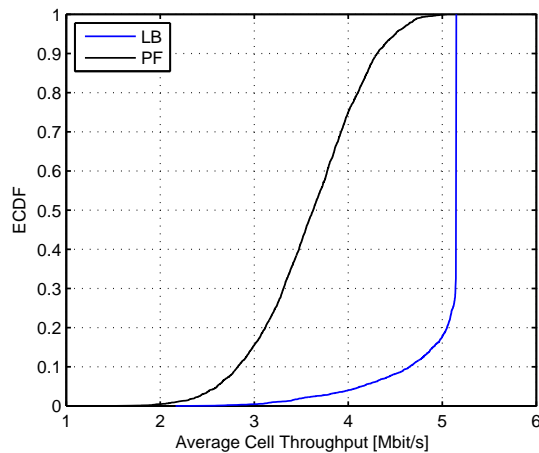

Figure 4.4: Cell throughput distributions of different scheduling algorithms

(a) Mean value

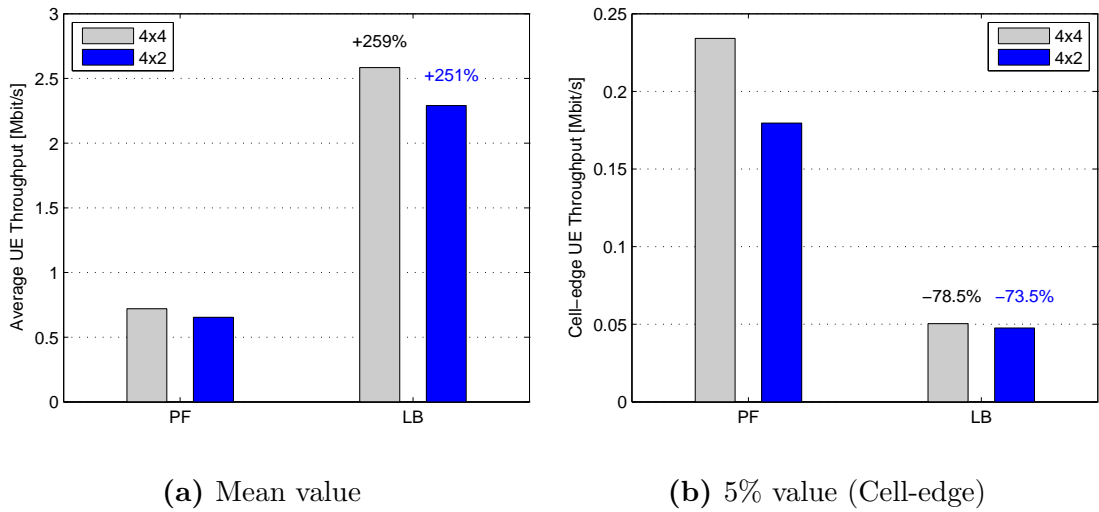**(b)** 5% value (Cell-edge)

Figure 4.5: UE throughput of different scheduling algorithms

Figure 4.6 (a) depicts the ASE of the two scheduling algorithms, showing a clear advantage of the LB algorithm (18% for 4, and 29% for 2 receive antennas). However, Figure 4.6 (b) evidently shows that the tradeoff for the high throughput of the LB scheduler is unfairness, Jain's Fairness Index (JFI) being close to the worst case of $0.2 = \frac{1}{5}$. This is because the LB algorithm only serves the UE with the best channel conditions, ignoring all other UEs.
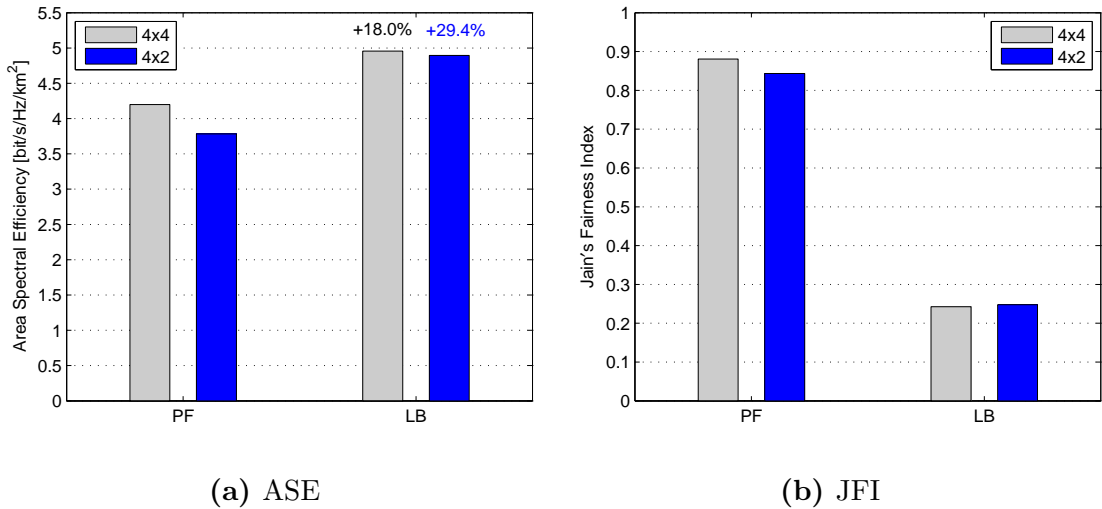

(a) ASE

(b) JFI

Figure 4.6: Additional performance comparisons

Chapter 5

Conclusion and Outlook

Throughout this thesis, cooperative transmission schemes for wireless cellular networks called Coordinated Scheduling (CS) and Coordinated Beamforming (CB) were investigated. They aim at suppressing the interference between adjacent cells in order to enhance the system throughput, especially at the cell edge.

The investigation begun by introducing the underlying framework, namely the LTE-A architecture and the corresponding system model. The subsequent chapters provided theoretical and mathematical descriptions of CS and CB algorithms. Their performance was then evaluated by means of physical-level simulations, utilizing the Vienna LTE-A Link Level Simulator.

The CB algorithms investigated in this thesis are ZIOP, LBP and Iterative beamforming. ZIOP is capable of completely removing ICI, leading to optimal results in high interference and low noise channels. However, in more realistic scenarios, ZIOP is performing highly suboptimal. LBP achieves an overall good performance. In 4×2 antenna setups, it suffers a slight loss, but still outperforms Non-CoMP schemes. The Iterative algorithm has clear strengths in 4×4 setups, but falls behind LBP when utilizing a 4×2 antenna configuration. The choice of a suitable CB scheme therefore heavily depends on the aspects of the considered system, such as SIR and SNR.

Regarding CS, the LB scheduling algorithm is studied and compared to the Non-CoMP PF scheduler. The LB scheduler is capable of achieving much higher cell throughputs than the PF scheduler, but does so at the expense of fairness, serving only few UEs that experience high channel quality.

The analyses conducted in this thesis assume perfect and a-priori channel knowledge at the transmitter. The future evaluations should investigate the impact of channel estimation errors on the performance gains achieved with CS and CB. In this context, the effects of feedback delay and UE mobility should be carefully considered. Further investigations regarding feedback and signaling overhead are

also necessary. And while simulations are a great way to check the feasibility of new algorithms, only measurements under realistic circumstances can evaluate their performance in a real system. For the use of CS and CB in commercial wireless communication systems, measurement-based evaluations are therefore necessary.

To conclude, it has been demonstrated that CS and CB have a considerable potential for improving cellular network performance. Now that these CoMP schemes are integrated into the LTE standard, there is no doubt about them having a huge impact on future wireless networks.

Appendix A

List of Abbreviations

3GPP	Third Generation Partnership Project
AMC	Adaptive Modulation and Coding
ASE	Area Spectral Efficiency
AWGN	Additive White Gaussian Noise
BLER	Block Error Ratio
CB	Coordinated Beamforming
CoMP	Coordinated Multi-Point
CQI	Channel Quality Indicator
CS	Coordinated Scheduling
DCS	Dynamic Cell Selection
ECDF	Empirical Cumulative Distribution Function
eNB	eNodeB
eNodeB	Evolved Base Station
FDD	Frequency Division Duplex
ICI	Inter-Cell Interference
ICIC	ICI Coordination
i.i.d.	independent and identically distributed
JFI	Jain's Fairness Index
JP	Joint Processing
JT	Joint Transmission
LB	Leakage-Based
LBP	LB Precoding
LTE	Long Term Evolution
LTE-A	LTE Advanced
MAC	Medium Access Control
MIESM	Mutual Information Effective SINR Mapping
MIMO	Multiple Input Multiple Output

MMSE	Minimum Mean-Squared Error
MSE	Mean-Squared Error
OFDM	Orthogonal Frequency Division Multiplexing
PF	Proportional Fair
QAM	Quadratur Amplitude Modulation
RB	Resource Block
RE	Resource Element
SINR	Signal-to-Interference-plus-Noise Ratio
SIR	Signal-to-Interference Ratio
SLNR	Signal-to-Leakage-plus-Noise Ratio
SNR	Signal-to-Noise Ratio
SVD	Singular Value Decomposition
TTI	Transmission Time Interval
UE	User Equipment
ZIOP	Zero Interference by Orthogonal Precoding

Bibliography

[1] Cisco Systems Inc., "**Cisco visual networking index: Global mobile data traffic forecast update, 2013-2018**," White paper, 2014.

[2] 3GPP, "**Technical specification group radio access network; Evolved universal terrestrial radio access (E-UTRA) and Evolved universal terrestrial radio access network (E-UTRAN); Overall description; Stage 2 (Release 8)**," TS 36.300, 2009, `http://www.3gpp.org/DynaReport/36300.htm`.

[3] M. Sawahashi, Y. Kishiyama, A. Morimoto, D. Nishikawa, and M. Tanno, "**Coordinated multipoint transmission/reception techniques for LTE-advanced**," *IEEE Wireless Commun.*, vol. 17, no. 3, pp. 26-34, 2010.

[4] J. Lee, Y. Kim, H. Lee, B.L. Ng, D. Mazzarese, J. Liu, W. Xiao, and Y. Zhou, "**Coordinated multipoint transmission and reception in LTE-advanced systems**," *IEEE Commun. Magazine*, vol. 50, no.11, pp. 44-50, 2012.

[5] 3GPP, "**Technical specification group radio access network; Coordinated multi-point operation for LTE physical layer aspects (Release 11)**," TR 36.819, 2013, `http://www.3gpp.org/DynaReport/36819.htm`.

[6] F. Rashid-Farrokhi, K.J.R. Liu, and L. Tassiulas, "**Transmit beamforming and power control for cellular wireless systems**," *IEEE J. Sel. Areas Commun.*, vol. 16, no. 8, pp. 1437-1450, 1998.

[7] S. Das, H. Viswanathan, and G. Rittenhouse, "**Dynamic load balancing through coordinated scheduling in packet data systems**," *IEEE INFO-COM 2003*, vol. 1, pp. 786-796, 2003.

[8] U. Jang, H. Son, J. Park, and S. Lee, "**CoMP-CSB for ICI nulling with user selection**," *IEEE Trans. Wireless Commun.*, vol. 10, no. 9, pp. 2982-2993, 2011.

[9] L. Qiang, Y. Yang, F. Shu, and W. Gang, "**Coordinated beamforming in downlink CoMP transmission system**," in *Proc. 5th Int. Conf. Commun. Netw. China*, pp. 1-5, 2010.

[10] E. Pateromichelakis, M. Shariat, A. ul Quddus, and R. Tafazolli, "**On the evolution of multi-cell scheduling in 3GPP LTE / LTE-A**," *IEEE Commun. Surveys and Tutorials*, vol. 15, no. 2, pp. 701-717, 2013.

[11] C. Mehlführer, J. C. Ikuno, M. Simko, S. Schwarz, and M. Rupp, "**The Vienna LTE simulators - Enabling reproducibility in wireless communications research**," *EURASIP JASP; Special Issue on Reproducible Research*, vol. 2011, no. 1, p. 29, 2011.

[12] **LTE Advanced Link Level Simulator**, `http://www.nt.tuwien.ac.at/research/mobile-communications/lte-simulators`, [Online; accessed 04/30/2014].

[13] S. Caban, C. Mehlführer, M. Rupp, and M. Wrulich, **Evaluation of HSDPA and LTE: From Testbed Measurements to System Level Performance.** UK: John Wiley & Sons, 2012.

[14] S. Ahmadi, **LTE-Advanced: A Practical Systems Approach to Understanding 3GPP LTE Releases 10 and 11 Radio Access Technologies**. Elsevier Science, 2013.

[15] 3GPP, "**Technical specification group radio access network; Evolved universal terrestrial radio access (E-UTRA); Physical channels and modulation (Release 11)**," TS 36.211, 2013, `http://www.3gpp.org/DynaReport/36211.htm`.

[16] 3GPP, "**Technical specification group radio access network; Evolved universal terrestrial radio access (E-UTRA); Base station radio transmission and reception (Release 11)**," TS 36.104, 2014, `http://www.3gpp.org/DynaReport/36104.htm`.

[17] S. Schwarz and M. Rupp, "**Throughput maximizing feedback for MIMO OFDM based wireless communication systems**," in *IEEE 12th International Workshop on SPAWC*, pp. 316-320, 2011.

[18] S. Schwarz, M. Wrulich, and M. Rupp, "**Mutual information based calculation of the precoding matrix indicator for 3GPP UMTS/LTE**," in *2010 International ITG WSA*, pp. 52-58, 2010.

[19] J. Ikuno, M. Wrulich, and M. Rupp, "**System level simulation of LTE networks**,", in *Proc. 71st Vehicular Technology Conference*, pp. 1-5, 2010.

[20] 3GPP, "**Technical specification group radio access network; Evolved universal terrestrial radio access (E-UTRA); Physical layer procedures (Release 11)**," TS 36.213, 2014, `http://www.3gpp.org/DynaReport/36213.htm`.

[21] C.E. Shannon, "**A mathematical theory of communication**," *The Bell system technical journal*, vol. 27, pp. 379-423, 1948.

[22] Q. Spencer, A. Swindlehurst, and M. Haardt, "**Zero-forcing methods for downlink spatial multiplexing in multiuser MIMO channels**," *IEEE Trans. on Signal Processing*, vol. 52, no. 2, pp. 461-471, 2004.

[23] V. Cadambe and S. Jafar, "**Interference alignment and degrees of freedom of the K-user interference channel**," *IEEE Trans. on Information Theory*, vol. 54, no. 8, pp. 3425-3441, 2008.

[24] S. Schwarz and M. Rupp, "**Exploring coordinated multipoint beamforming strategies**," submitted for review on *IEEE Access*, 2014.

[25] M. Sadek, A. Tarighat, and A. Sayed, "**A leakage-based precoding scheme for downlink multi-user MIMO channels**," *IEEE Trans. Wireless Commun.*, vol. 6, no. 5, pp. 1711-1721, 2007.

[26] H. Wang, S. Yan, D. Xu, X. Tang, and T. Huang, "**Trace ratio vs. ratio trace for dimensionality reduction**," in *IEEE Conference on CVPR*, pp. 1-8, 2007.

[27] Motorola, "**SCF-based coordinated beamforming and performance gain over single-point SU/MU beamforming**," R1-094848, 3GPP TSG RAN1#59, 2009.

[28] M. Rupp, "**Robust design of adaptive equalizers**," *IEEE Trans. on Signal Processing*, vol. 60, no. 4, pp. 1612-1626, 2012.

[29] T.K. Moon, W.C. Stirling, **Mathematical Methods and Algorithms for Signal Processing**. Prentice Hall, 2000.

[30] 3GPP, "**Technical specification group radio access network; Deployment aspects (Release 8)**," TR 25.943, 2008, `http://www.3gpp.org/DynaReport/25943.htm`.

[31] M.-S. Alouini and A. Goldsmith, "**Area spectral efficiency of cellular mobile radio systems**," *IEEE Trans. on Vehicular Technology*, vol. 48, no. 4, pp. 1047-1066, 1999.

[32] R. Heath, Jr., T. Wu, Y.H. Kwon, and A.C.K. Soong, "**Multiuser MIMO in distributed antenna systems with out-of-cell interference**," *IEEE Trans. on Signal Processing*, vol. 59, no. 10, 2011.

[33] Nokia Siemens Networks, Nokia, "**Coordinated beamforming/scheduling performance evaluation**," R1-100331, 3GPP TSG RANWG1 Meeting #59b, 2010.

[34] P. Viswanath, D.N.C. Tse, and R. Laroia, "**Opportunistic beamforming using dumb antennas**," *IEEE Trans. on Info. Theory*, vol. 48, no. 6, pp. 1277-1294, 2002.

[35] R. Jain, D. Chiu, and W. Hawe, "**A Quantitative Measure of Fairness and Discrimination for Resource Allocation in Shared Computer Systems**," DEC, Tech. Rep. TR-301, 1984.